



Resource Allocation in Spectrum-Sharing Cognitive Heterogeneous Networks

19

Haijun Zhang, Theodoros A. Tsiftsis, Julian Cheng,
and Victor C. M. Leung

Contents

Introduction	636
Sensing Time Optimization and Power Control for Energy-Efficient Cognitive Small Cell with Imperfect Hybrid Spectrum Sensing	637
System Model and Problem Formulation	638
Energy-Efficient Resource Optimization in One Cognitive Small Cell	643
Energy-Efficient Resource Optimization in Multiple Cognitive Small Cells	648
Simulation Results and Discussion	651
Interference-Limited Resource Optimization in Cognitive Femtocells with Fairness and Imperfect Spectrum Sensing	659
System Model	659
Optimization Framework with Imperfect Spectrum Sensing	661
Joint Resource Optimization with Fairness and Imperfect Sensing	664
Simulation Results and Discussions	670
Conclusion	676

H. Zhang (✉)

Beijing Engineering and Technology Research Center for Convergence Networks and Ubiquitous Services, University of Science and Technology Beijing, Beijing, China

e-mail: haijunzhang@ieee.org

T. A. Tsiftsis

School of Engineering, Nazarbayev University, Astana, Akmola, Kazakhstan

e-mail: theodoros.tsiftsis@nu.edu.kz

J. Cheng

School of Engineering, The University of British Columbia, Kelowna, BC, Canada

e-mail: julian.cheng@ubc.ca

V. C. M. Leung

Department of Electrical and Computer Engineering, The University of British Columbia, Vancouver, BC, Canada

e-mail: vleung@ece.ubc.ca

Appendix	676
References	678
Further Reading	680

Abstract

Cognitive radio-enabled heterogeneous networks are an emerging technology to address the exponential increase of mobile traffic demand in the next-generation mobile communications. Recently, many technological issues such as resource allocation and interference mitigation pertaining to cognitive heterogeneous networks have been studied, but most studies focus on maximizing spectral efficiency. This chapter introduces the resource allocation problem in cognitive heterogeneous networks, where the cross-tier interference mitigation, imperfect spectrum sensing, and energy efficiency are considered. The optimization of power allocation is formulated as a non-convex optimization problem, which is then transformed to a convex optimization problem. An iterative power control algorithm is developed by considering imperfect spectrum sensing, cross-tier interference mitigation, and energy efficiency.

Keywords

Cognitive heterogeneous networks · Fairness · Imperfect spectrum sensing · Orthogonal frequency division multiple access (OFDMA) · Power control · Resource allocation Sensing time optimization

Introduction

Demand for mobile data traffic is increasing exponentially due to the wide usage of smart mobile devices and data-centric applications in mobile Internet. As a promising technology in the fifth-generation (5G) mobile communications, small cell can offload heavy traffics from primary macrocells by shortening the distance between basestation and users. Since small cell can effectively improve the coverage and spatial reuse of spectrum by deploying low-power access points, it is not surprising that small cell has attracted much research interests in both industry and academia. However, the benefits of small cell deployments come with a number of fundamental challenges, which include spectrum access, resource allocation, and interference mitigation [1–7].

Cognitive radio is also an emerging technology to improve the efficiency of spectrum access in the 5G networks [8]. The cognitive capabilities can improve the spectrum efficiency, radio resource utilization, and interference mitigation by efficient spectrum sensing, interference sensing, and adaptive transmission. Therefore, a cognitive radio-enabled small cell network can further improve the system performance by coexisting with a macrocell network [9]. There are three ways for a cognitive small cell to access the spectrum potentially used by a primary macrocell: (1) spectrum sharing, where the cognitive small cell can share the

spectrum with the primary macrocell; (2) opportunistic spectrum access, where the cognitive small cell can opportunistically access the spectrum that is detected to be idle; and (3) hybrid spectrum sensing, where the cognitive small cell senses the channel status and optimizes the power allocation based on the spectrum sensing result.

Orthogonal frequency division multiple access (OFDMA) working jointly with cognitive small cell can improve spectrum efficiency and energy efficiency via resource allocation and interference mitigation [10]. In [11], the authors investigated the resource allocation problems based on multistage stochastic programming for stringent quality of service (QoS) requirements of real-time streaming scalable videos in cognitive small cell networks. The issues on spectrum sensing and interference mitigation were studied in [12], where an interference coordination approach was adopted. Opportunistic cooperation between cognitive small cell users and primary macrocell users was provided for cognitive small cell networks based on a generalized Lyapunov optimization technique [13]. In [14], a spectrum-sharing scheme between primary macrocell and secondary small cell was investigated, and bounds on maximum intensity of simultaneously transmitting cognitive small cell that satisfies a given per-tier outage constraint in these schemes were theoretically derived using a stochastic geometry model. In [15], interferences due to different interfering sources were analyzed within cognitive-empowered small cell networks, and a stochastic dual control approach was introduced for dynamic sensing coordination and interference mitigation without involving global and centralized control efforts. Moreover, energy-efficient resource allocation has also been investigated for cognitive radio and small cell. In [16], the energy efficiency aspect of spectrum sharing and power allocation was studied using a Stackelberg game in heterogeneous cognitive radio networks with femtocells. While in [17], Nash equilibrium of a power adaptation game was derived to reduce energy consumption. Moreover, interference temperature limits, originated from the cognitive radio, were used in [18] to mitigate cross-tier interferences between macrocell and small cell.

This chapter includes two parts. In the first part, the power control and sensing time optimization problem in a cognitive small cell network are discussed. The resource allocation problem is solved by two new algorithms. In the second part, an iterative subchannel and power allocation algorithm is applied to the cognitive femtocells. The effectiveness of the provided algorithm in terms of capacity and fairness when compared to the other existing algorithms is verified by simulation.

Sensing Time Optimization and Power Control for Energy-Efficient Cognitive Small Cell with Imperfect Hybrid Spectrum Sensing

In this part, we study the optimization of sensing time and power control in an OFDMA-based cognitive small cell by considering energy efficiency, QoS requirement, cross-tier interference limitation, and imperfect hybrid spectrum sensing.

System Model and Problem Formulation

System Model

We consider an OFDMA cognitive small cell network where a co-channel cognitive small cell is overlaid on a primary macrocell and focus on resource allocation in the downlink of the cognitive small cell. The OFDMA system has a bandwidth of B , which is divided into N subchannels. The channel fading of each subcarrier is assumed to be the same within a subchannel, but may vary across different subchannels. The channel model for each subchannel includes path loss and frequency-nonselctive Rayleigh fading. Before the small cell accesses the spectrum licensed to the primary macrocell, cognitive small basestation (CSBS) performs spectrum sensing to determine the occupation status of the subchannels. In each time frame, the cognitive small cell can sense N subchannels by energy detection-based spectrum sensing. The CSBS adapts the transmit power based on the spectrum sensing result [19]. The H_n^o is the hypothesis that the n th subchannel is occupied by the primary macrocell. The \mathcal{H}_n^o represents the spectrum sensing result that the n th subchannel is occupied by the primary macrocell. The H_n^v is the hypothesis that the n th subchannel is not occupied by the primary macrocell. The \mathcal{H}_n^v represents the spectrum sensing result that the n th subchannel is not occupied by the primary macrocell. The probabilities of false alarm and mis-detection on subchannel n are q_n^f and q_n^m , respectively. The user signal of the primary macrocell is a complex-valued phase shift keying (PSK) signal, and the noise at CSBS is circularly symmetric complex Gaussian (CSCG) with mean zero and variance σ^2 [19]. According to [20], the probability of mis-detection q_n^m can be approximated by

$$q_n^m(\varepsilon_n, \tau) = 1 - Q\left(\left(\frac{\varepsilon_n}{\sigma^2} - \gamma_n - 1\right) \sqrt{\frac{\tau f}{2\gamma_n + 1}}\right) \quad (1)$$

where ε_n is a chosen threshold of energy detector on subchannel n , τ is the spectrum sensing time, γ_n is the received signal-to-noise ratio (SNR) of the primary macrocell user measured at the CSBS on subchannel n , f is the sampling frequency, and the standard Gaussian Q -function is defined as

$$Q(x) = \frac{1}{\sqrt{2\pi}} \int_x^\infty \exp(-t^2/2) dt. \quad (2)$$

The probability of false alarm q_n^f can be approximated by [20]

$$\begin{aligned} q_n^f(\varepsilon_n, \tau) &= Q\left(\left(\frac{\varepsilon_n}{\sigma^2} - 1\right) \sqrt{\tau f}\right) \\ &= Q\left(\sqrt{2\gamma_n + 1} (Q^{-1}(\hat{q}_n^d)) + \sqrt{\tau f} \gamma_n\right) \end{aligned} \quad (3)$$

where \hat{q}_n^d is the target probability of detection.

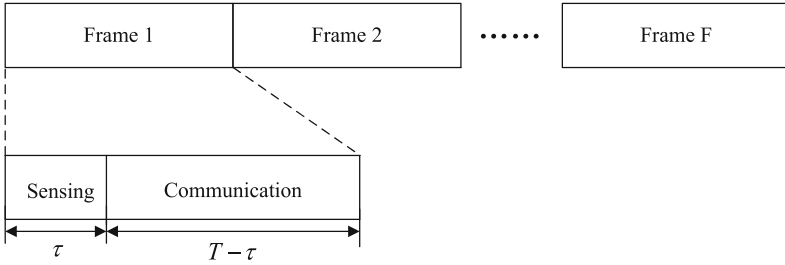


Fig. 1 The frame structure of cognitive small cell networks

The frame structure of the considered cognitive small cell network is shown in Fig. 1 [20]. As can be seen from Fig. 1, a spectrum sensing duration/time τ is inserted in the beginning of each frame. The CSBS adapts its transmit power based on the spectrum sensing decision made in the beginning of each frame. If the subchannel n is detected to be idle (\mathcal{H}_n^v), the cognitive small cell can transmit high-power $P_{s,n}^v$; if the subchannel n is detected to be occupied (\mathcal{H}_n^o), the cognitive small cell can transmit low-power $P_{s,n}^o$ in order to mitigate the interference caused to the primary macrocell. This approach is called hybrid spectrum sensing, and it is different from the opportunistic spectrum access and the spectrum-sharing approach. Based on the Shannon’s capacity formula, when the spectrum sensing result is idle, the achievable capacity on subchannel n in the small cell is given by [19]

$$R_{v,n} = \log_2 \left(1 + \frac{g_{ss,n} \cdot P_{s,n}^v}{\sigma^2} \right) \tag{4}$$

where $g_{ss,n}$ is the channel gain of subchannel n between the small cell user and CSBS. If the spectrum sensing result is active/occupied, the achievable capacity on subchannel n in the small cell is given by [19]

$$R_{o,n} = \log_2 \left(1 + \frac{g_{ss,n} \cdot P_{s,n}^o}{g_{ms,n} \cdot P_{m,n}^o + \sigma^2} \right) \tag{5}$$

where $g_{ms,n}$ is the channel gain of subchannel n between the macrocell basestation (MBS) and CSBS and $P_{m,n}^o$ is the transmit power of MBS on subchannel n .

In a cognitive heterogeneous network, which typically consists of a cognitive small cell and a primary macrocell, imperfect spectrum sensing of CSBS can cause severe co-channel interference to the primary macrocell and thus degrade the performance of the heterogeneous cognitive small cell networks [19]. Since it is the CSBS that determines whether a subchannel is occupied by the primary

macrocell or not, according to [19], four different cases are to be considered as follows.

- Case 1: subchannel n is vacant in primary macrocell, and the spectrum sensing decision made by CSBS is vacant;
- Case 2: subchannel n is vacant in primary macrocell, but the spectrum sensing decision made by CSBS is occupied;
- Case 3: subchannel n is occupied in primary macrocell, but the spectrum sensing decision made by CSBS is vacant;
- Case 4: subchannel n is occupied in primary macrocell, and the spectrum sensing decision made by CSBS is occupied.

For the first and fourth cases, the CSBS makes the correct decisions. On the other hand, the second case is false alarm, and the third case is mis-detection. Therefore, the achievable capacities on subchannel n in small cell can be calculated for the four different cases as [19]

$$R_{1,n} = \log_2 \left(1 + \frac{g_{ss,n} \cdot P_{s,n}^v}{\sigma^2} \right), \quad (6)$$

$$R_{2,n} = \log_2 \left(1 + \frac{g_{ss,n} \cdot P_{s,n}^o}{\sigma^2} \right), \quad (7)$$

$$R_{3,n} = \log_2 \left(1 + \frac{g_{ss,n} \cdot P_{s,n}^v}{g_{ms,n} \cdot P_{m,n} + \sigma^2} \right), \quad (8)$$

$$R_{4,n} = \log_2 \left(1 + \frac{g_{ss,n} \cdot P_{s,n}^o}{g_{ms,n} \cdot P_{m,n} + \sigma^2} \right). \quad (9)$$

Our objective is to maximize energy efficiency of cognitive small cell networks by optimizing sensing time and power allocation. The energy efficiencies of those four cases [19] are defined as follows:

$$\eta_{1,n} = \frac{R_{1,n}}{P_{s,n}^v + P_c}, \quad (10)$$

$$\eta_{2,n} = \frac{R_{2,n}}{P_{s,n}^o + P_c}, \quad (11)$$

$$\eta_{3,n} = \frac{R_{3,n}}{P_{s,n}^v + P_c}, \quad (12)$$

$$\eta_{4,n} = \frac{R_{4,n}}{P_{s,n}^o + P_c} \quad (13)$$

where P_c is the constant circuit power consumption which includes lowpass filter, mixer for modulation, frequency synthesizer, and digital-to-analog converter [21] and P_c is assumed to be independent of the transmitted power [22].

The average energy efficiency of subchannel n in the hybrid spectrum sensing scheme is [19]

$$\begin{aligned} \eta_n = & P(\mathcal{H}_n^v) \left(1 - q_n^f(\varepsilon_n, \tau)\right) \eta_{1,n} \\ & + P(\mathcal{H}_n^v) q_n^f(\varepsilon_n, \tau) \eta_{2,n} \\ & + P(\mathcal{H}_n^o) q_n^m(\varepsilon_n, \tau) \eta_{3,n} \\ & + P(\mathcal{H}_n^o) \left(1 - q_n^m(\varepsilon_n, \tau)\right) \eta_{4,n} \end{aligned} \quad (14)$$

where $P(\mathcal{H}_n^v)$ and $P(\mathcal{H}_n^o)$ are the probabilities of vacant status and occupied status of subchannel n , respectively.

Since the resource allocation is performed in CSBS, the transmit power of CSBS on subchannel n is constrained by [19]

$$\sum_{n=1}^N \left[\begin{array}{l} P(\mathcal{H}_n^v) \left(1 - q_n^f(\varepsilon_n, \tau)\right) P_{s,n}^v \\ + P(\mathcal{H}_n^v) q_n^f(\varepsilon_n, \tau) P_{s,n}^o \\ + P(\mathcal{H}_n^o) q_n^m(\varepsilon_n, \tau) P_{s,n}^v \\ + P(\mathcal{H}_n^o) \left(1 - q_n^m(\varepsilon_n, \tau)\right) P_{s,n}^o \end{array} \right] \frac{T - \tau}{T} \leq P_{\max} \quad (15)$$

where P_{\max} is the maximum average transmit power of CSBS.

Since primary macrocells play a fundamental role in providing cellular coverage, macrocell users' QoS should not be affected by cognitive small cell's deployment. Therefore, to implement cross-tier interference protection, an average interference power limit is imposed to constrain the cross-tier interference suffered by macrocell [19]. Let I_n^{th} denote the maximum tolerable interference level on subchannel n for the macrocell user. We have

$$P(\mathcal{H}_n^o) \cdot g_{sm,n} \left[\begin{array}{l} q_n^m(\varepsilon_n, \tau) P_{s,n}^v + \\ \left(1 - q_n^m(\varepsilon_n, \tau)\right) P_{s,n}^o \end{array} \right] \frac{T - \tau}{T} \leq I_n^{th}, \forall n \quad (16)$$

where $g_{sm,n}$ is the channel power gain from the small cell to the macrocell user on subchannel n .

In order to guarantee the QoS for the small cell, a minimum transmit data rate constraint is introduced as [19]

$$\begin{aligned} & P(\mathcal{H}_n^v) \left(1 - q_n^f(\varepsilon_n, \tau)\right) R_{1,n} + P(\mathcal{H}_n^v) q_n^f(\varepsilon_n, \tau) R_{2,n} \\ & + P(\mathcal{H}_n^o) q_n^m(\varepsilon_n, \tau) R_{3,n} + P(\mathcal{H}_n^o) \left(1 - q_n^m(\varepsilon_n, \tau)\right) R_{4,n} \geq R_{\min} \end{aligned} \quad (17)$$

where R_{\min} is the minimum transmit data rate requirement of each subchannel.

For a target detection probability of \widehat{q}_n^d on subchannel n , substituting \widehat{q}_n^d into (1), we obtain

$$\left(\frac{\varepsilon_n}{\sigma^2} - \gamma_n - 1\right) \sqrt{\frac{\tau f}{2\gamma_n + 1}} = Q^{-1}(\widehat{q}_n^d). \quad (18)$$

Therefore, for a given sensing time $\widehat{\tau}$, the detection threshold ε_n can be determined as

$$\varepsilon_n = \left(\sqrt{\frac{2\gamma_n + 1}{\widehat{\tau} f}} Q^{-1}(\widehat{q}_n^d) + \gamma_n + 1\right) \sigma^2, \forall n. \quad (19)$$

Problem Formulation

In this part, the aim is to maximize the cognitive small cell's energy efficiency while protecting QoS of the primary macrocell users. The cross-tier interference power limit is sent by a primary MBS periodically. This process requires little overhead in the primary macrocell. In this case, the sensing time optimization and power control in primary macrocell are not part of optimization [19]. Thus, the corresponding sensing time optimization and power allocation problem for the downlink CSBS can be mathematically formulated as [19]

$$\max_{\{\tau, P_{s,n}^v, P_{s,n}^o\}} \sum_{n=1}^N \frac{T - \tau}{T} \eta_n(\tau, P_{s,n}^v, P_{s,n}^o) \quad (20)$$

s.t.

$$C1: \sum_{n=1}^N \left[P(\mathcal{H}_n^v)(1 - q_n^f(\varepsilon_n, \tau))P_{s,n}^v + P(\mathcal{H}_n^v)q_n^f(\varepsilon_n, \tau)P_{s,n}^o \right. \\ \left. + P(\mathcal{H}_n^o)q_n^m(\varepsilon_n, \tau)P_{s,n}^v + P(\mathcal{H}_n^o)(1 - q_n^m(\varepsilon_n, \tau))P_{s,n}^o \right] \frac{T - \tau}{T} \leq P_{\max}$$

$$C2: P(\mathcal{H}_n^o) \cdot g_{sm,n} [q_n^m(\varepsilon_n, \tau)P_{s,n}^v + (1 - q_n^m(\varepsilon_n, \tau))P_{s,n}^o] \frac{T - \tau}{T} \leq I_n^{th}, \forall n$$

$$C3: P(\mathcal{H}_n^v)(1 - q_n^f(\varepsilon_n, \tau))R_{1,n} + P(\mathcal{H}_n^v)q_n^f(\varepsilon_n, \tau)R_{2,n} \\ + P(\mathcal{H}_n^o)q_n^m(\varepsilon_n, \tau)R_{3,n} + P(\mathcal{H}_n^o)(1 - q_n^m(\varepsilon_n, \tau))R_{4,n} \geq R_{\min}, \forall n$$

$$C4: P_{s,n}^v \geq 0, P_{s,n}^o \geq 0, \forall n$$

$$C5: 0 \leq \tau \leq T$$

(21)

where $\mathbf{P}_s^v = [p_{s,n}^v]_{1 \times N}$ and $\mathbf{P}_s^o = [p_{s,n}^o]_{1 \times N}$ are the power allocation vectors of the N subchannels in the cognitive small cell. In (21), $C1$ limits the maximum transmit power of each CSBS to P_{\max} ; $C2$ sets the tolerable interference power level on each subchannel of the macrocell user on subchannel n ; $C3$ represents minimum QoS requirement of each subchannel; $C4$ represents the nonnegative power constraint of the transmit power on each subchannel; $C5$ expresses the constraint of sensing time in each frame.

Note that the optimization problem in (20) under the constraints of (21) is non-convex with respect to $\{\tau, \mathbf{P}_s^v, \mathbf{P}_s^o\}$ [19]. Therefore, the problem of energy-efficient power control is investigated given the sensing time $\hat{\tau}$.

Energy-Efficient Resource Optimization in One Cognitive Small Cell

Transformation of the Optimization Problem

Given the sensing time $\hat{\tau}$, the power control problem in (20) under the constraints of (21) can be classified as a nonlinear fractional programming problem. Since the joint optimization problem of \mathbf{P}_s^v and \mathbf{P}_s^o in (20) can be decoupled into two separate subproblems, namely, one for \mathbf{P}_s^v and the other for \mathbf{P}_s^o [19]. The subproblem related to \mathbf{P}_s^v is first solved. Since subchannels in (20) are independent, a nonnegative variable $\eta_{13,n}^*$ is defined for the sum of average energy efficiencies on subchannel n in Case 1 and Case 3 as [19]

$$\eta_{13,n}^* = \frac{\left\{ \begin{array}{l} P(\mathcal{H}_n^v)(1 - q_n^f(\varepsilon_n, \hat{\tau}))R_{1,n}(\hat{\tau}, \tilde{P}_{s,n}^v) \\ + P(\mathcal{H}_n^o)q_n^m(\varepsilon_n, \hat{\tau})R_{3,n}(\hat{\tau}, \tilde{P}_{s,n}^v) \end{array} \right\}}{\tilde{P}_{s,n}^v + P_c} \tag{22}$$

where $\tilde{P}_{s,n}^v$ is the optimal solution to the problem of (20) under the constraints of (21).

Theorem 1. $\eta_{13,n}^*$ is achieved if and only if (80) where the $P_{s,n}^v$ in (80) is one of the feasible solutions to (20) under the constraints of (21).

The proof is provided in Appendix.

According to the Theorem 1, the objective function with respect to \mathbf{P}_s^o in fractional form can also be transformed to a subtractive form by introducing a nonnegative variable $\eta_{24,n}^*$.

Iterative Energy Efficiency Maximization Algorithm

To solve the transformed optimization problem in the subtractive form under the constraints of (20), Algorithm 1 [19] is provided.

Algorithm 1 Energy-efficient power control algorithm

```

1: Initialize the maximum number of iterations  $L_{\max}$  and convergence tolerance  $\varepsilon_\eta$ ;
2: Set  $\eta_{13,n}(1) = 0, \eta_{24,n}(1) = 0, l = 0$ ;
3: Initialize power allocation with an equal power distribution and begin the outer loop;
4: for  $n = 1$  to  $N$  do
5:   repeat
6:     a) The inner loop power control problem is solved with outer loop results  $\eta_{13,n}^*(l)$ ,
        $\eta_{24,n}^*(l)$ , the Lagrangian method and (28), (31);
7:     b) Then, the power control solution  $\underline{P}_{s,n}^v(l)$  and  $\underline{P}_{s,n}^o(l)$  can be obtained;
8:     if  $(P(\mathcal{H}_n^v)(1 - q_n^f(\varepsilon_n, \hat{\tau}))R_{1,n}(\hat{\tau}, \underline{P}_{s,n}^v(l)) + P(\mathcal{H}_n^o)q_n^m(\varepsilon_n, \hat{\tau})R_{3,n}(\hat{\tau}, \underline{P}_{s,n}^v(l)) -$ 
        $\eta_{13,n}(l)(\underline{P}_{s,n}^v(l) + P_c)) < \varepsilon_\eta$  then
9:       Convergence= true;  $\tilde{P}_{s,n}^v = \underline{P}_{s,n}^v(l)$ 
10:       $\eta_{13,n}^* =$ 
       
$$\frac{P(H_n^v)(1 - q_n^f(\varepsilon_n, \hat{\tau}))R_{1,n}(\hat{\tau}, \tilde{P}_{s,n}^v) + P(H_n^o)q_n^m(\varepsilon_n, \hat{\tau})R_{3,n}(\hat{\tau}, \tilde{P}_{s,n}^v)}{\tilde{P}_{s,n}^v + P_c}$$

11:     else
12:       $\eta_{13,n}(l+1) =$ 
       
$$\frac{P(H_n^v)(1 - q_n^f(\varepsilon_n, \hat{\tau}))R_{1,n}(\hat{\tau}, \underline{P}_{s,n}^v(l)) + P(H_n^o)q_n^m(\varepsilon_n, \hat{\tau})R_{3,n}(\hat{\tau}, \underline{P}_{s,n}^v(l))}{\underline{P}_{s,n}^v(l) + P_c}$$

13:     Convergence= false,  $l = l + 1$ ;
14:     end if
15:     if  $(P(\mathcal{H}_n^v)q_n^f(\varepsilon_n, \hat{\tau})R_{2,n}(\hat{\tau}, \underline{P}_{s,n}^o(l)) + P(\mathcal{H}_n^o)(1 - q_n^m(\varepsilon_n, \hat{\tau}))R_{4,n}(\hat{\tau}, \underline{P}_{s,n}^o(l)) -$ 
        $\eta_{24,n}(l)(\underline{P}_{s,n}^o(l) + P_c)) < \varepsilon_\eta$  then
16:       Convergence= true;  $\tilde{P}_{s,n}^o = \underline{P}_{s,n}^o(l)$ 
17:       $\eta_{24,n}^* =$ 
       
$$\frac{P(H_n^v)q_n^f(\varepsilon_n, \hat{\tau})R_{2,n}(\hat{\tau}, \tilde{P}_{s,n}^o) + P(H_n^o)(1 - q_n^m(\varepsilon_n, \hat{\tau}))R_{4,n}(\hat{\tau}, \tilde{P}_{s,n}^o)}{\tilde{P}_{s,n}^o + P_c}$$

18:     else
19:       $\eta_{24,n}(l+1) =$ 
       
$$\frac{P(H_n^v)q_n^f(\varepsilon_n, \hat{\tau})R_{2,n}(\hat{\tau}, \underline{P}_{s,n}^o(l)) + P(H_n^o)(1 - q_n^m(\varepsilon_n, \hat{\tau}))R_{4,n}(\hat{\tau}, \underline{P}_{s,n}^o(l))}{\underline{P}_{s,n}^o(l) + P_c}$$

20:     Convergence= false,  $l = l + 1$ ;
21:     end if
22:   until Convergence= true or  $l = L_{\max}$ 
23: end for

```

As shown in Algorithm 1, in each iteration of the outer loop, the l th inner loop power control problem is given as

$$\max_{\{P_s^v, P_s^o\}} \sum_{n=1}^N \frac{T - \hat{\tau}}{T} \left\{ \begin{array}{l} P(\mathcal{H}_n^v)(1 - q_n^f(\varepsilon_n, \hat{\tau}))R_{1,n}(\hat{\tau}, P_{s,n}^v) \\ + P(\mathcal{H}_n^o)q_n^m(\varepsilon_n, \hat{\tau})R_{3,n}(\hat{\tau}, P_{s,n}^v) \\ + P(\mathcal{H}_n^v)q_n^f(\varepsilon_n, \hat{\tau})R_{2,n}(\hat{\tau}, P_{s,n}^v) \\ + P(\mathcal{H}_n^o)(1 - q_n^m(\varepsilon_n, \hat{\tau}))R_{4,n}(\hat{\tau}, P_{s,n}^o) \\ - \eta_{13,n}(l)(P_{s,n}^v + P_c) \\ - \eta_{24,n}(l)(P_{s,n}^o + P_c) \end{array} \right\} \quad (23)$$

$$\text{s.t. } C1 - C4. \quad (24)$$

Since the optimization problem of (23) under the constraints of (24) is convex with respect to \mathbf{P}_s^v and \mathbf{P}_s^o . The Lagrangian function is given by (25)

$$\begin{aligned}
L(\mathbf{P}_s^v, \mathbf{P}_s^o, \lambda, \boldsymbol{\mu}, \mathbf{v}) = & \\
& \left\{ \sum_{n=1}^N \frac{T-\hat{\tau}}{T} \left[\begin{aligned} & (P(\mathcal{H}_n^v)(1-q_n^f(\varepsilon_n, \hat{\tau}))R_{1,n}(\hat{\tau}, P_{s,n}^v) \\ & + P(\mathcal{H}_n^o)q_n^m(\varepsilon_n, \hat{\tau})R_{3,n}(\hat{\tau}, P_{s,n}^v) - \eta_{13,n}(l)P_{s,n}^v \\ & + P(\mathcal{H}_n^v)q_n^f(\varepsilon_n, \hat{\tau})R_{2,n}(\hat{\tau}, P_{s,n}^o) \\ & + P(\mathcal{H}_n^o)(1-q_n^m(\varepsilon_n, \hat{\tau}))R_{4,n}(\hat{\tau}, P_{s,n}^o) - \eta_{24,n}(l)P_{s,n}^o \end{aligned} \right] \right\} \\
& - \lambda \left\{ \sum_{n=1}^N \left[\begin{aligned} & P(\mathcal{H}_n^v)(1-q_n^f(\varepsilon_n, \hat{\tau}))P_{s,n}^v + P(\mathcal{H}_n^v)q_n^f(\varepsilon_n, \hat{\tau})P_{s,n}^o + \\ & P(\mathcal{H}_n^o)q_n^m(\varepsilon_n, \hat{\tau})P_{s,n}^v + P(\mathcal{H}_n^o)(1-q_n^m(\varepsilon_n, \hat{\tau}))P_{s,n}^o \end{aligned} \right] \frac{T-\hat{\tau}}{T} - P_{\max} \right\} \\
& - \sum_{n=1}^N \mu_n \left\{ \sum_{n=1}^N P(\mathcal{H}_n^o)g_{sm,n}(q_n^m(\varepsilon_n, \hat{\tau}))P_{s,n}^v + (1-q_n^m(\varepsilon_n, \hat{\tau}))P_{s,n}^o \right\} \frac{T-\hat{\tau}}{T} - I_n^{th} \left\} \\
& + \sum_{n=1}^N v_n \left\{ \left[\begin{aligned} & P(\mathcal{H}_n^v)(1-q_n^f(\varepsilon_n, \tau))R_{1,n} + P(\mathcal{H}_n^v)q_n^f(\varepsilon_n, \tau)R_{2,n} \\ & + P(\mathcal{H}_n^o)q_n^m(\varepsilon_n, \tau)R_{3,n} + P(\mathcal{H}_n^o)(1-q_n^m(\varepsilon_n, \tau))R_{4,n} \end{aligned} \right] - R_{\min} \right\} \quad (25)
\end{aligned}$$

where λ , $\boldsymbol{\mu}_n$, and \mathbf{v}_n are the Lagrangian multipliers (also called dual variables) vectors for the constraints C1, C2, and C3 in (21), respectively. Thus, the Lagrangian dual function is [19] defined as

$$g(\lambda, \boldsymbol{\mu}, \mathbf{v}) = \max_{\mathbf{P}_s^v, \mathbf{P}_s^o} L(\mathbf{P}_s^v, \mathbf{P}_s^o, \lambda, \boldsymbol{\mu}, \mathbf{v}). \quad (26)$$

The dual problem can be expressed as [19]

$$\min_{\lambda, \boldsymbol{\mu}, \mathbf{v} \geq 0} g(\lambda, \boldsymbol{\mu}, \mathbf{v}). \quad (27)$$

Using Lagrangian function and the Karush-Kuhn-Tucker (KKT) conditions, the near optimal solution of $\tilde{P}_{s,n}^v$ on subchannel n can be obtained as

$$\tilde{P}_{s,n}^v = \left[\frac{A_{v,n} + \sqrt{B_{v,n}}}{2} \right]^+ \quad (28)$$

where $[x]^+ = \max\{x, 0\}$, and $A_{v,n}$ and $B_{v,n}$ are given by (29) and (30), respectively.

$$\begin{aligned}
A_{v,n} = & \frac{(1+v_n)(P(\mathcal{H}_n^v)(1-q_n^f(\varepsilon_n, \hat{\tau})) + P(\mathcal{H}_n^o)q_n^m(\varepsilon_n, \hat{\tau}))}{\ln 2(\eta_{13,n}(l) + \lambda(P(\mathcal{H}_n^v)(1-q_n^f(\varepsilon_n, \hat{\tau})) + P(\mathcal{H}_n^o)q_n^m(\varepsilon_n, \hat{\tau}))} \\ & + \mu_n g_{sm,n} P(\mathcal{H}_n^o)q_n^m(\varepsilon_n, \hat{\tau})) \\ & - \frac{2\sigma^2 + g_{ms,n}P_{m,n}^o}{g_{ss,n}} \quad (29)
\end{aligned}$$

$$B_{v,n} = A_{v,n}^2 - \frac{4}{g_{ss,n}} \cdot \left\{ \frac{\sigma^4 + \sigma^2 g_{ms,n} P_{m,n}^o}{g_{ss,n}} \right. \\ \left. \frac{(1 + v_n)[P(\mathcal{H}_n^v)(1 - q_n^f(\varepsilon_n, \hat{\tau})(\sigma^2 + g_{ms,n} P_{m,n}^o)) + P(\mathcal{H}_n^o)q_n^m(\varepsilon_n, \hat{\tau})\sigma^2]}{\ln 2(\eta_{13,n}(l) + \lambda(P(\mathcal{H}_n^v)(1 - q_n^f(\varepsilon_n, \hat{\tau}) + P(\mathcal{H}_n^o)q_n^m(\varepsilon_n, \hat{\tau})) + \mu_n g_{sm,n} P(\mathcal{H}_n^o)q_n^m(\varepsilon_n, \hat{\tau})))} \right\}. \quad (30)$$

Similar to $\tilde{P}_{s,n}^v$, the near optimal solution of $\tilde{P}_{s,n}^o$ on subchannel n can be obtained as

$$\tilde{P}_{s,n}^o = \left[\frac{A_{o,n} + \sqrt{B_{o,n}}}{2} \right]^+ \quad (31)$$

$$A_{o,n} = \frac{(1 + v_n)(P(\mathcal{H}_n^v)q_n^f(\varepsilon_n, \hat{\tau}) + P(\mathcal{H}_n^o)(1 - q_n^m(\varepsilon_n, \hat{\tau})))}{\ln 2(\eta_{24,n}(l) + \lambda(P(\mathcal{H}_n^v)q_n^f(\varepsilon_n, \hat{\tau}) + P(\mathcal{H}_n^o)(1 - q_n^m(\varepsilon_n, \hat{\tau}))) + \mu_n g_{sm,n} P(\mathcal{H}_n^o)(1 - q_n^m(\varepsilon_n, \hat{\tau})))} \\ - \frac{2\sigma^2 + g_{ms,n} P_{m,n}^o}{g_{ss,n}} \quad (32)$$

$$B_{o,n} = A_{o,n}^2 - \frac{4}{g_{ss,n}} \cdot \left\{ \frac{\sigma^4 + \sigma^2 g_{ms,n} P_{m,n}^o}{g_{ss,n}} \right. \\ \left. \frac{(1 + v_n)[P(\mathcal{H}_n^v)q_n^f(\varepsilon_n, \hat{\tau})(\sigma^2 + g_{ms,n} P_{m,n}^o) + P(\mathcal{H}_n^o)(1 - q_n^m(\varepsilon_n, \hat{\tau}))\sigma^2]}{\ln 2(\eta_{13,n}(l) + \lambda(P(\mathcal{H}_n^v)q_n^f(\varepsilon_n, \hat{\tau}) + P(\mathcal{H}_n^o)(1 - q_n^m(\varepsilon_n, \hat{\tau}))) + \mu_n g_{sm,n} P(\mathcal{H}_n^o)(1 - q_n^m(\varepsilon_n, \hat{\tau})))} \right\}. \quad (33)$$

where $A_{o,n}$ and $B_{o,n}$ are given by (32) and (33), respectively.

Either the ellipsoid or the subgradient method can be adopted in updating the dual variables [23]. Here, the subgradient method is chosen to update the dual variables, and the update formulas are (34), (35), and (36)

$$\lambda^{l+1} = \lambda^l - \vartheta_1^l \left(P_{\max} - \sum_{n=1}^N \left[\frac{P(\mathcal{H}_n^v)(1 - q_n^f(\varepsilon_n, \tau))P_{s,n}^v + P(\mathcal{H}_n^o)q_n^f(\varepsilon_n, \tau)P_{s,n}^o}{P(\mathcal{H}_n^o)q_n^m(\varepsilon_n, \tau)P_{s,n}^v + P(\mathcal{H}_n^o)(1 - q_n^m(\varepsilon_n, \tau))P_{s,n}^o} \right] \frac{T - \tau}{T} \right) \quad (34)$$

$$\mu_n^{l+1} = \mu_n^l - \vartheta_2^l \left(I_n^{th} - P(\mathcal{H}_n^o) \cdot g_{sm,n} [q_n^m(\varepsilon_n, \tau)P_{s,n}^v + (1 - q_n^m(\varepsilon_n, \tau))P_{s,n}^o] \frac{T - \tau}{T} \right), \forall n \quad (35)$$

$$v_n^{l+1} = v_n^l - \vartheta_3^l \left(\left\{ \frac{P(\mathcal{H}_n^v)(1 - q_n^f(\varepsilon_n, \tau))R_{1,n} + P(\mathcal{H}_n^v)q_n^f(\varepsilon_n, \tau)R_{2,n} + P(\mathcal{H}_n^o)q_n^m(\varepsilon_n, \tau)R_{3,n} + P(\mathcal{H}_n^o)(1 - q_n^m(\varepsilon_n, \tau))R_{4,n}}{T} - R_{\min} \right\}, \forall n \right) \quad (36)$$

where ϑ_1^l , ϑ_2^l , and ϑ_3^l denote the step size of iteration l ($l \in \{1, 2, \dots, L_{\max}\}$) for λ , μ , and ν , respectively, and L_{\max} is the maximum number of iterations. Meanwhile, the step size must meet the following conditions

$$\sum_{l=1}^{\infty} \vartheta_i^l = \infty, \lim_{l \rightarrow \infty} \vartheta_i^l = 0, \forall i \in \{1, 2, 3\}. \quad (37)$$

Algorithm 1 is provided to optimize the power $P_{s,n}^v$ and $P_{s,n}^o$ of (20) given the sensing time $\hat{\tau}$ [19]. In Algorithm 1, the process of power control is decomposed to inner loop problem and outer loop problem. In each iteration, both $\eta_{13,n}^*(l)$ and $\eta_{24,n}^*(l)$ can be found through outer loop, the inner loop control problem is solved by the outer loop results $\eta_{13,n}^*(l)$ and $\eta_{24,n}^*(l)$, the Lagrangian method and (28), (31).

The near optimal sensing time scheme can be found in Algorithm 2 [19] based on a one-dimensional exhaustive search.

Algorithm 2 is provided to optimize the sensing time in (20) when the optimal power through Algorithm 1 has been obtained. Therefore, running Algorithm 1 with $\hat{\tau}(l)$ to obtain the optimal power $\tilde{P}_{s,n}^v$ and $\tilde{P}_{s,n}^o$ has to be firstly done in Algorithm 2. Then the optimal sensing time is found based on a one-dimensional exhaustive search.

Complexity Analysis

The computational complexity of the provided algorithms is analyzed in this subsection. Suppose the subgradient method used in Algorithm 1 requires Δ_1 iterations to converge; the updates of λ need $O(1)$ operations; μ and ν need $O(N)$ operations each. The method used in Algorithm 1 to calculate $\eta_{13,n}^*$ and $\eta_{24,n}^*$ on each subchannel in a small cell needs Δ_2 iterations to converge. The total complexity of Algorithm 1 is thus $O(N^2\Delta_1\Delta_2)$. The parameters Δ_1 and Δ_2 can be small enough if the initial values of λ , μ and ν are well chosen, together with suitable

Algorithm 2 Near optimal energy-efficient sensing time scheme

- 1: Initialize the maximum number of iterations L_{\max} and convergence tolerance ε_τ
 - 2: Set $l = 0$; Initialize $\hat{\tau}(l)$;
 - 3: **repeat**
 - 4: Run Algorithm 1 with $\hat{\tau}(l)$ to obtain the optimal power $\tilde{P}_{s,n}^v$ and $\tilde{P}_{s,n}^o$;
 - 5: $P_{s,n}^v(l) = \tilde{P}_{s,n}^v$, $P_{s,n}^o(l) = \tilde{P}_{s,n}^o$;
 - 6: $\hat{\tau}(l) = \max_{\tau} \sum_{n=1}^N \frac{T-\tau}{T} \eta_n(\tau, P_{s,n}^v(l), P_{s,n}^o(l))$;
 - 7: **if** $|\hat{\tau}(l) - \hat{\tau}(l-1)| \leq \varepsilon_\tau$ **then**
 - 8: Convergence= **true**, $\tilde{\tau} = \hat{\tau}(l)$;
 - 9: **else**
 - 10: Convergence= **false**, $l = l + 1$;
 - 11: **end if**
 - 12: **until** Convergence= **true** or $l = L_{\max}$
-

values of iteration step sizes. In Algorithm 2, finding the optimal sensing time for each subchannel requires $O(L)$ operations. Therefore, the total computational complexity of Algorithm 2 is $O(NL)$ for the network with N subchannels [19].

Energy-Efficient Resource Optimization in Multiple Cognitive Small Cells

Multiple Cognitive Small Cells Scenario

In this subsection, the energy-efficient resource optimization is investigated in multiple cognitive small cells. The aforementioned method is applied to optimize the energy efficiency in multiple cognitive small cells network, where the interference between small cells will be considered. In multiple cognitive small cells, to maximize the total energy efficiency with the consideration of co-tier interference mitigation, the problem in (20) under the constraints of (21) can be formulated as [19]

$$\begin{aligned}
 & \max_{\{\tau, \mathbf{P}_{\text{ms}}^v, \mathbf{P}_{\text{ms}}^o\}} \sum_{k=1}^K \sum_{n=1}^N \frac{T - \tau_k}{T} \eta_{k,n}(\tau_k, P_{s,k,n}^v, P_{s,k,n}^o) \quad (38) \\
 \text{s.t. } C1: & \sum_{n=1}^N \left[P(\mathcal{H}_{k,n}^v)(1 - q_{k,n}^f(\varepsilon_{k,n}, \tau_k))P_{s,k,n}^v + P(\mathcal{H}_{k,n}^v)q_{k,n}^f(\varepsilon_{k,n}, \tau_k)P_{s,k,n}^o \right. \\
 & \left. + P(\mathcal{H}_{k,n}^o)q_{k,n}^m(\varepsilon_{k,n}, \tau_k)P_{s,k,n}^v + P(\mathcal{H}_{k,n}^o)(1 - q_{k,n}^m(\varepsilon_{k,n}, \tau_k))P_{s,k,n}^o \right] \\
 & \times \frac{T - \tau_k}{T} \leq P_{\text{max}} \\
 C2: & P(H_{k,n}^o) \cdot g_{k,n}^{sm} [q_{k,n}^m(\varepsilon_{k,n}, \tau_k)P_{s,k,n}^v + (1 - q_{k,n}^m(\varepsilon_{k,n}, \tau_k))P_{s,k,n}^o] \frac{T - \tau_k}{T} \\
 & \leq I_{k,n}^{th}, \forall k, n \\
 C3: & P(\mathcal{H}_{k,n}^v)(1 - q_{k,n}^f(\varepsilon_{k,n}, \tau_k))R_{k,n}^1 + P(\mathcal{H}_{k,n}^v)q_{k,n}^f(\varepsilon_{k,n}, \tau_k)R_{k,n}^2 \\
 & + P(\mathcal{H}_{k,n}^o)q_{k,n}^m(\varepsilon_{k,n}, \tau_k)R_{k,n}^3 + P(\mathcal{H}_{k,n}^o)(1 - q_{k,n}^m(\varepsilon_{k,n}, \tau_k))R_{k,n}^4 \geq R_{\text{min}} \\
 C4: & \sum_{j=1, j \neq k}^K \frac{T - \tau_k}{T} g_{k,j,n} \\
 & \left\{ P(\mathcal{H}_{j,n}^o) \left[q_{j,n}^m(\varepsilon_{j,n}, \tau_j)P_{s,j,n}^v + (1 - q_{j,n}^m(\varepsilon_{j,n}, \tau_j))P_{s,j,n}^o \right] + \right. \\
 & \left. P(\mathcal{H}_{j,n}^v) \left[q_{j,n}^f(\varepsilon_{j,n}, \tau_j)P_{s,j,n}^o + (1 - q_{j,n}^f(\varepsilon_{j,n}, \tau_j))P_{s,j,n}^v \right] \right\} \\
 & \leq \gamma_{k,n}^{th}, \forall n, k \\
 C5: & P_{s,k,n}^v \geq 0, P_{s,k,n}^o \geq 0, \forall n, k \\
 C6: & 0 \leq \tau_k \leq T, \forall k
 \end{aligned}$$

(39)

where $\boldsymbol{\tau} = [\tau]_{1 \times K}$ is the sensing time vector of K cognitive small cells, N is the number of subchannels in each small cell, and $\mathbf{P}_{\text{ms}}^v = [P_{s,k,n}^v]_{K \times N}$ and $\mathbf{P}_{\text{ms}}^o = [P_{s,k,n}^o]_{K \times N}$ are the power allocation vectors of the N subchannels in K cognitive small cells. Constraint $C1$ limits the maximum transmit power of each CSBS to P_{max} ; $C2$ sets the tolerable interference power level for each small cell on each subchannel of the macrocell user on subchannel n ; $C3$ represents minimum QoS requirement of each subchannel; $C4$ represents the tolerable interference power level from other small cells, where $\gamma_{k,n}^{th}$ denotes the co-tier interference limits on the n th subchannel in the k th small cell; $C5$ represents the nonnegative power constraint of the transmit power on each subchannel; $C6$ expresses the constraint of sensing time in each frame.

First of all, similar to the problem in (20), the problem of power control in (38) under the constraints of (39) can be decoupled into two separate subproblems respect to \mathbf{P}_{ms}^v and \mathbf{P}_{ms}^o , respectively, when the sensing time $\hat{\tau}_k$ is given. The subproblem respect to \mathbf{P}_{ms}^v is dealt with [19]. The variable $\eta_{k,n}^{13*}$ is defined as

$$\eta_{k,n}^{13*} = \frac{P(\mathcal{H}_{k,n}^v)(1 - q_{k,n}^f(\varepsilon_{k,n}, \hat{\tau}_k))R_{k,n}^1(\hat{\tau}_k, \tilde{P}_{s,k,n}^v) + P(\mathcal{H}_{k,n}^o)q_{k,n}^m(\varepsilon_{k,n}, \hat{\tau}_k)R_{k,n}^3(\hat{\tau}_k, \tilde{P}_{s,k,n}^v)}{\tilde{P}_{s,k,n}^v + P_c} \quad (40)$$

where $\eta_{k,n}^{13*}$ represents the sum of average energy efficiencies on the n th subchannel of the k th small cell in Case 1 and Case 3. $\tilde{P}_{s,k,n}^v$ is the optimal solution to the problem of (38) under the constraints of (39).

Therefore, the optimization problem of (38) is transformed as optimization problem of (40) under the constraints of (39) [19]. Subsequently, Algorithm 1 is used to solve the transformed problem [19], and the near optimal solution can be obtained [19]

$$\tilde{P}_{s,k,n}^v = \left[\frac{A_{v,k,n} + \sqrt{B_{v,k,n}}}{2} \right]^+ \quad (41)$$

where $A_{v,k,n}$ and $B_{v,k,n}$ are given by

$$A_{v,k,n} = \frac{(1 + v_{k,n})(P(\mathcal{H}_{k,n}^v)(1 - q_{k,n}^f(\varepsilon_{k,n}, \hat{\tau}_k)) + P(\mathcal{H}_{k,n}^o)q_{k,n}^m(\varepsilon_{k,n}, \hat{\tau}_k))}{\left\{ \begin{array}{l} \ln 2 \left(\eta_{k,n}^{13} (l) + \lambda_{k,n} \left(P(\mathcal{H}_{k,n}^v) \left(1 - q_{k,n}^f(\varepsilon_{k,n}, \hat{\tau}_k) \right) \right. \right. \\ \left. \left. + P(\mathcal{H}_{k,n}^o) q_{k,n}^m(\varepsilon_{k,n}, \hat{\tau}_k) \right) + \mu_{k,n} g_{k,n}^{sm} P(\mathcal{H}_{k,n}^o) q_{k,n}^m(\varepsilon_{k,n}, \hat{\tau}_k) \right) \\ \left. - \xi_{k,n} \sum_{j=1, j \neq k}^K g_{j,k,n} \left[P(\mathcal{H}_{j,n}^v) \left(1 - q_{j,n}^f(\varepsilon_{j,n}, \hat{\tau}_j) \right) \right. \right. \\ \left. \left. + P(\mathcal{H}_{j,n}^o) q_{j,n}^m(\varepsilon_{j,n}, \hat{\tau}_j) \right] \right\}} - \frac{2\sigma^2 + g_{k,n}^{ms} P_{m,n}^o}{g_{k,n}^{ss}} \quad (42)$$

$$B_{v,k,n} = A_{v,k,n}^2 \left\{ \frac{4}{g_{k,n}^{ss}} \left[\frac{\sigma^4 + \sigma^2 g_{k,n}^{ms} P_{m,k,n}^o}{g_{k,n}^{ss}} \right. \right. \\
 \left. \left. \frac{(1 + v_{k,n}) [P(\mathcal{H}_{k,n}^v)(1 - q_{k,n}^f(\varepsilon_{k,n}, \hat{\tau}_k))(\sigma^2 + g_{k,n}^{ms} P_{m,k,n}^o) + P(\mathcal{H}_{k,n}^o)q_{k,n}^m(\varepsilon_{k,n}, \hat{\tau}_k)\sigma^2]}{\left(\begin{array}{l} \ln 2(\eta_{k,n}^{13}(l) + \lambda_k(P(\mathcal{H}_{k,n}^v)(1 - q_{k,n}^f(\varepsilon_{k,n}, \hat{\tau}_k)) + P(\mathcal{H}_{k,n}^o)q_{k,n}^m(\varepsilon_{k,n}, \hat{\tau}_k)) \\ + \mu_{k,n}g_{k,n}^{ms}P(\mathcal{H}_{k,n}^o)q_{k,n}^m(\varepsilon_{k,n}, \hat{\tau}_k) \\ - \xi_{k,n} \sum_{j=1, j \neq k}^K g_{j,k,n} [P(\mathcal{H}_{j,n}^v)(1 - q_{j,n}^f(\varepsilon_{j,n}, \hat{\tau}_j)) + P(\mathcal{H}_{j,n}^o)q_{j,n}^m(\varepsilon_{j,n}, \hat{\tau}_j)] \end{array} \right)} \right] \right\} \quad (43)$$

Similar to $\tilde{P}_{s,k,n}^v$, the near optimal solution can be obtained

$$\tilde{P}_{s,k,n}^o = \left[\frac{A_{o,k,n} + \sqrt{B_{o,k,n}}}{2} \right]^+ \quad (44)$$

where $A_{o,k,n}$ and $B_{o,k,n}$ are given by (45) and (46), respectively.

$$A_{o,k,n} = \frac{(1 + v_{k,n})P(\mathcal{H}_{k,n}^v)q_{k,n}^f(\varepsilon_{k,n}, \hat{\tau}_k) + P(\mathcal{H}_{k,n}^o)(1 - q_{k,n}^m(\varepsilon_{k,n}, \hat{\tau}_k))}{\left(\begin{array}{l} \ln 2(\eta_{k,n}^{24}(l) + \lambda_{k,n}P(\mathcal{H}_{k,n}^v)q_{k,n}^f(\varepsilon_{k,n}, \hat{\tau}_k) \\ + P(\mathcal{H}_{k,n}^o)(1 - q_{k,n}^m(\varepsilon_{k,n}, \hat{\tau}_k)) + \mu_{k,n}g_{k,n}^{sm}P(\mathcal{H}_{k,n}^o)(1 - q_{k,n}^m(\varepsilon_{k,n}, \hat{\tau}_k)) \\ - \xi_{k,n} \sum_{j=1, j \neq k}^K g_{j,k,n} \left[\begin{array}{l} P(\mathcal{H}_{j,n}^v)q_{j,n}^f(\varepsilon_{j,n}, \hat{\tau}_j) \\ + P(\mathcal{H}_{j,n}^o)(1 - q_{j,n}^m(\varepsilon_{j,n}, \hat{\tau}_j)) \end{array} \right] \end{array} \right)} \\
 - \frac{2\sigma^2 + g_{k,n}^{ms}P_{m,n}^o}{g_{k,n}^{ss}} \quad (45)$$

$$B_{o,k,n} = A_{o,k,n}^2 \left(\frac{4}{g_{k,n}^{ss}} \left[\frac{\sigma^4 + \sigma^2 g_{k,n}^{ms} P_{m,k,n}^o}{g_{k,n}^{ss}} \right. \right. \\ \left. \left. \frac{(1 + v_{k,n}) [P(\mathcal{H}_{k,n}^v) q_{k,n}^f(\varepsilon_{k,n}, \hat{\tau}_k) (\sigma^2 + g_{k,n}^{ms} P_{m,k,n}^o) + P(\mathcal{H}_{k,n}^o) (1 - q_{k,n}^m(\varepsilon_{k,n}, \hat{\tau}_k)) \sigma^2]}{\left(\begin{array}{l} \ln 2 (\eta_{k,n}^{13})^3 (l) + \lambda_k (P(\mathcal{H}_{k,n}^v) q_{k,n}^f(\varepsilon_{k,n}, \hat{\tau}_k) + P(\mathcal{H}_{k,n}^o) (1 - q_{k,n}^m(\varepsilon_{k,n}, \hat{\tau}_k)) \\ + \mu_{k,n} g_{k,n}^{ms} P(\mathcal{H}_{k,n}^o) (1 - q_{k,n}^m(\varepsilon_{k,n}, \hat{\tau}_k)) \\ - \xi_{k,n} \sum_{j=1, j \neq k}^K g_{j,k,n} [P(\mathcal{H}_{j,n}^v) q_{j,n}^f(\varepsilon_{j,n}, \hat{\tau}_j) + P(\mathcal{H}_{j,n}^o) (1 - q_{j,n}^m(\varepsilon_{j,n}, \hat{\tau}_j))] \end{array} \right)} \right] \right) \quad (46)$$

Finally, the near optimal sensing time for each small cell can be found in Algorithm 2 based on a one-dimensional exhaustive search [19].

Complexity Analysis

In this part, the computational complexity of the provided algorithms in multiple small cells network is analyzed. Similar to the single small cell case, suppose the subgradient method used in Algorithm 1 needs Δ_1 iterations to converge; the updates of λ need $O(N)$ operations; μ and ν need $O(KN)$ operations each. The method used in Algorithm 1 to calculate $\eta_{13,n}^*$ and $\eta_{24,n}^*$ on each subchannel in a small cell needs Δ_2 iterations to converge. The total complexity of Algorithm 1 is thus $O(N^2 K^2 \Delta_1 \Delta_2)$. The parameters Δ_1 and Δ_2 can be small enough if the values of iteration step sizes and initial values of λ , μ , and ν are well chosen. In Algorithm 2, finding the optimal sensing time for each subchannel requires $O(L)$ operations. Therefore, the total computational complexity of Algorithm 2 is $O(KNL)$.

Simulation Results and Discussion

In this part, simulation results are presented to evaluate the performance of the provided algorithms. The sampling frequency f is 6 MHz, $T = 0.1$ s, $N = 50$, and $\sigma^2 = 1 \times 10^{-4}$. The channel gains are modeled as block faded and exponentially

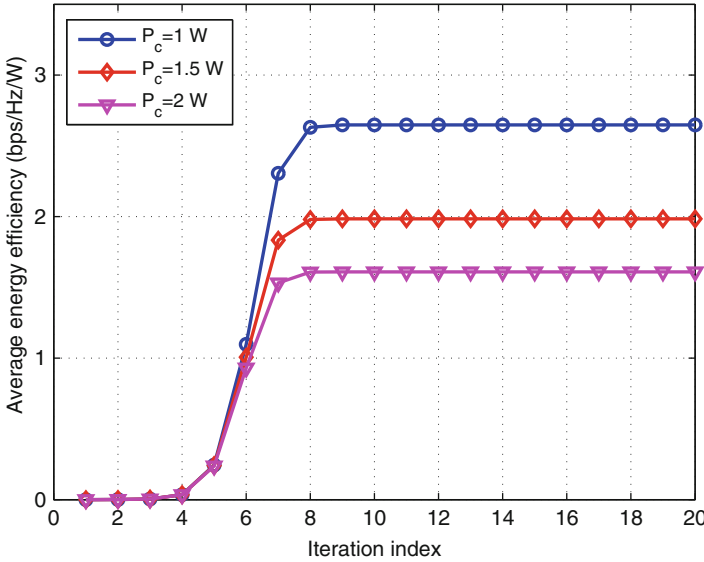


Fig. 2 Convergence in terms of average energy efficiency of small cell on each subchannel versus the number of iterations

distributed with mean of 0.1. The transmit power on each subchannel of primary macrocell is set at 25 mW. The QoS requirement of minimum data rate requirement is set as 0.3 bps/Hz. The target detection probability \hat{q}_n^d is set as 90% unless otherwise specified [19].

In Fig. 2, the convergence of Algorithm 1 is evaluated with the $P_{\max} = 15$ dBm, the cross-tier interference limit $I_n^{th} = -10$ dBm. As can be seen from Fig. 2, the average energy efficiency of small cell on each subchannel converges after nine iterations. This result, together with the previous analysis, indicates that the provided Algorithm 1 is practical in cognitive small cell [19].

Figure 3 displays the average energy efficiency of each subchannel in cognitive small cell network when the sensing time increases from 0.0005 to 0.015 s with $P_{\max} = 5, 10, 13, 15$ dBm, the cross-tier interference limit $I_n^{th} = -10$ dBm. The relation between sensing time and the average energy efficiency of each subchannel is exhibited [19]. As shown in Fig. 3, the average energy efficiency of each subchannel in cognitive small cell first increases and then drops when the sensing time is increased from 0.0005 to 0.015 s. It is estimated that the near optimal sensing time is between 0.002 and 0.004 s. Larger value of P_{\max} results in higher average energy efficiency because a larger value of P_{\max} enlarges the feasible region of the variables in the original optimization problem in (20)–(21).

Figure 4 shows the trend of average energy efficiency of each subchannel in cognitive small cell when P_{\max} increases from 5 to 25 dBm [19]. The target detection probabilities $\hat{q}_n^d = 0.8, 0.9$ and cross-tier interference limit $I_n^{th} = -10$ dBm in Fig. 4. As shown in Fig. 4, the average energy efficiency of each subchannel of

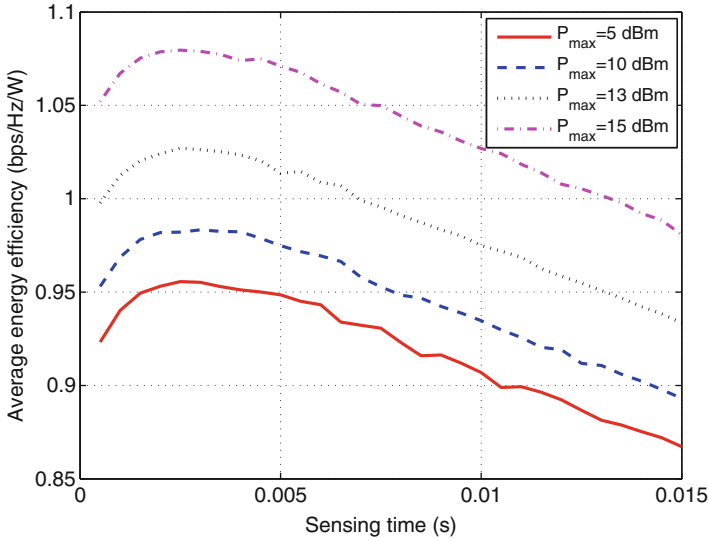


Fig. 3 Average energy efficiency versus sensing time with different P_{\max} values

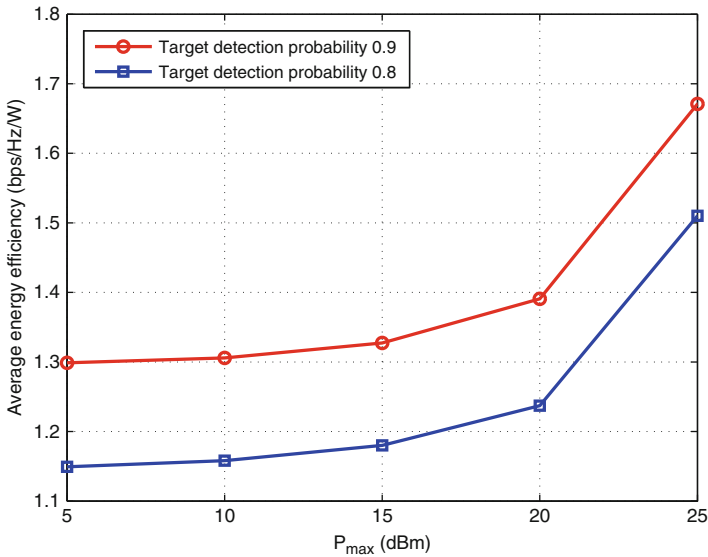


Fig. 4 Average energy efficiency versus P_{\max} with different target detection probabilities

cognitive small cell increases when P_{\max} is increased from 5 to 25 dBm, because a larger value of P_{\max} results in a larger optimal power in (20)–(21). A larger target detection probability which results in better performance of the optimal average energy efficiency from Fig. 4 can be seen. The reason is that a larger target detection probability makes it more accurate in detection of spectrum sensing [19].

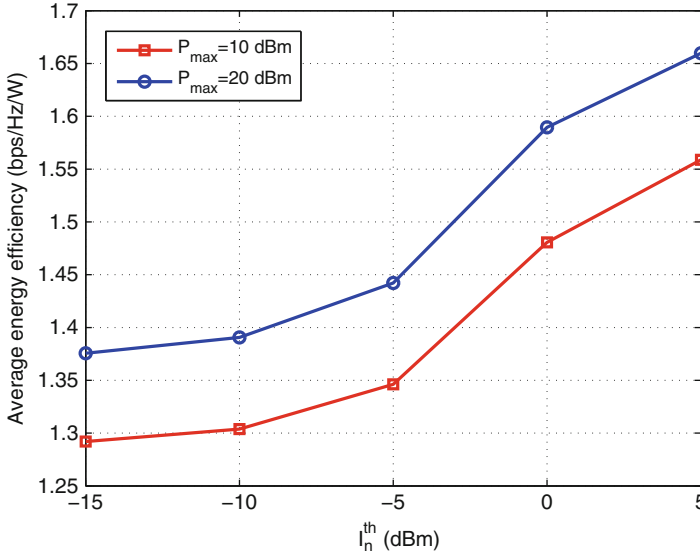


Fig. 5 Average energy efficiency versus the cross-tier interference limit with different P_{max} values

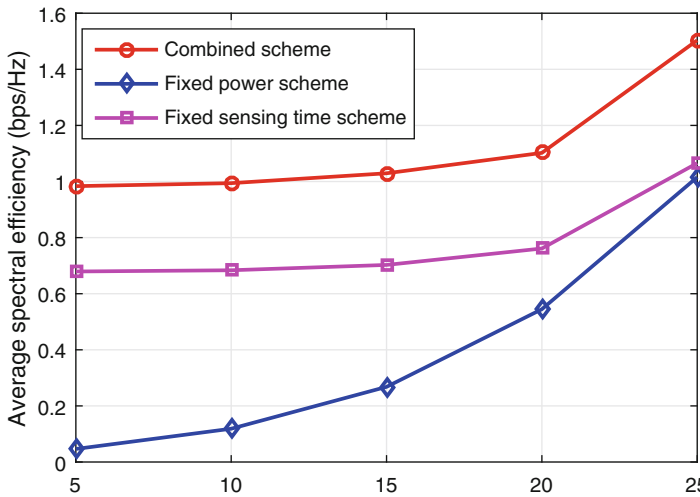


Fig. 6 Performance comparison of different schemes in terms of average spectral efficiency of small cell on each subchannel

Figure 5 shows the relation between cross-tier interference limit and the average energy efficiency of each subchannel with a different target detection probability. As shown in Fig. 5, the average energy efficiency of each subchannel in cognitive small cell increases when I_n^{th} is changed from -15 to 5 dBm. Similar to Fig. 3, this is because that a larger value of I_n^{th} can enlarge the feasible region of the optimizing variable of power in (20)–(21).

Figure 6 shows the performance comparison of average spectral efficiency with different schemes. The combined scheme is the combination of the provided Algorithm 1 and the provided near optimal sensing time scheme. Fixed sensing time scheme is the combination of the provided Algorithm 1 and a random selected sensing time scheme. Fixed power scheme is the combination of equal power allocation and the provided optimal sensing time scheme [19]. As shown in Fig. 6, the average spectral efficiency of each subchannel in the cognitive small cell with P_{\max} increases from 5 to 25 mW. However, the combined scheme outperforms the fixed sensing time scheme and the fixed power scheme obviously.

Figure 7 provides the energy efficiency performance comparison between combined scheme and the other methods. In Fig. 7, the average energy efficiency of each subchannel in the cognitive small cell is shown when P_{\max} increases from 8 to 18 mW, where the target detection probability $\hat{q}_n^d = 0.9$ and cross-tier interference limit $I_n^{th} = -10$ dBm. As shown in Fig. 7, the combined scheme can achieve 15% higher energy efficiency than the fixed sensing time scheme. Fixed power scheme has the lowest curve, because of equal power allocation [19].

Figure 8 shows the relation between cross-tier interference limit and the optimal sensing time. As shown in Fig. 8, the near optimal sensing time decreases with an increase of I_n^{th} . Because when using KKT conditions related to C2, larger I_n^{th} results in larger optimized sensing time. Moreover, a larger value of P_{\max} results in smaller optimized sensing time.

Figure 9 shows the relation between the sensing time and average energy efficiency of each subchannel in cognitive small cell network with a different cross-tier interference limit. As shown in Fig. 9, similar to Fig. 3, the average energy efficiency of each subchannel in cognitive small cell first increases and then drops as the sensing time is increased from 0.0005 to 0.015 s. It is because that the near

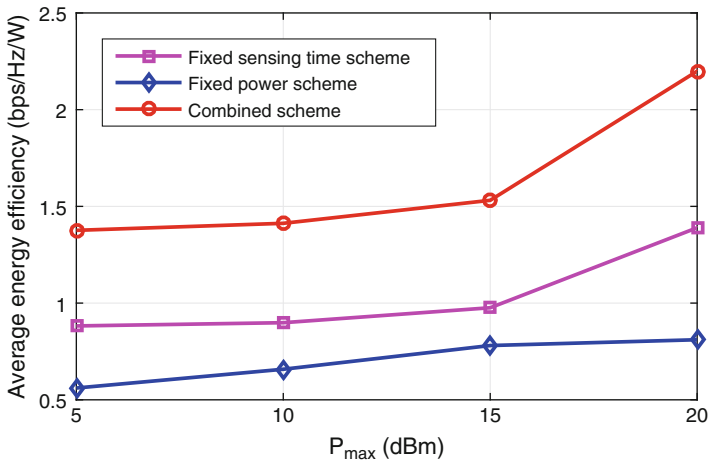


Fig. 7 Performance comparison of different schemes in terms of average energy efficiency of small cell on each subchannel

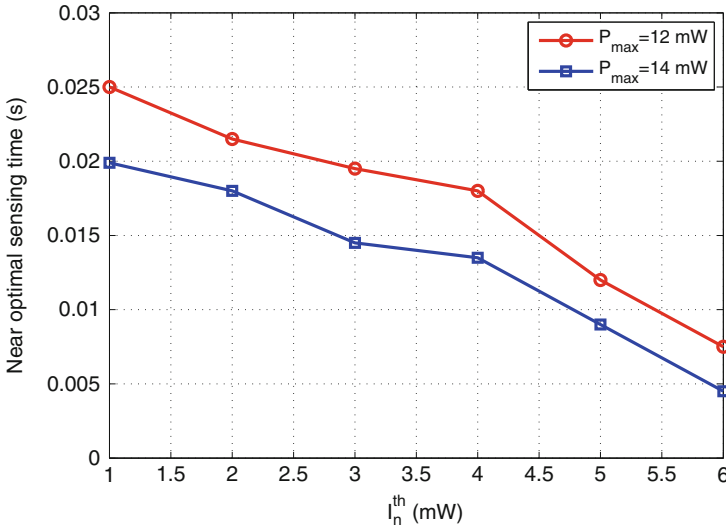


Fig. 8 Near optimal sensing time versus the cross-tier interference limit with different P_{max} values

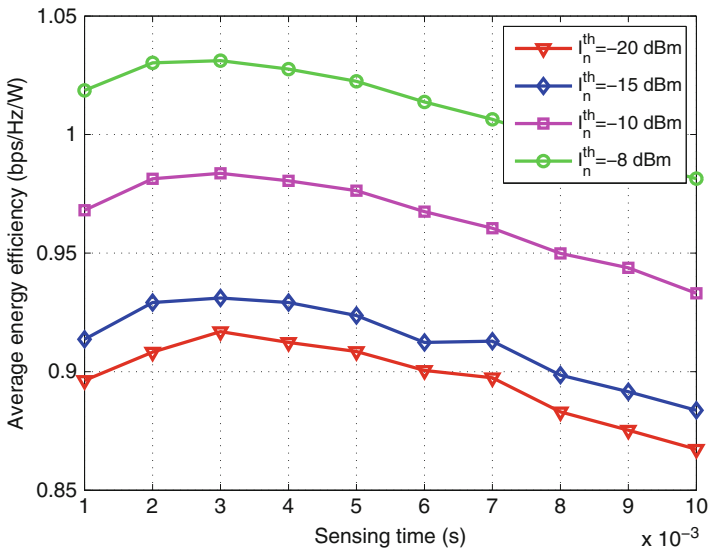


Fig. 9 Average energy efficiency versus sensing time with different cross-tier interference limits

optimal sensing time is between 0.002 and 0.004 s. Larger I_n^{th} value results in higher average energy efficiency since a larger value of I_n^{th} leads to a larger optimization variable region in (20)–(21) [19].

Figure 10 displays the trend of average energy efficiency of each subchannel in cognitive small cell when P_{max} increases from 5 to 25 dBm with cross-tier

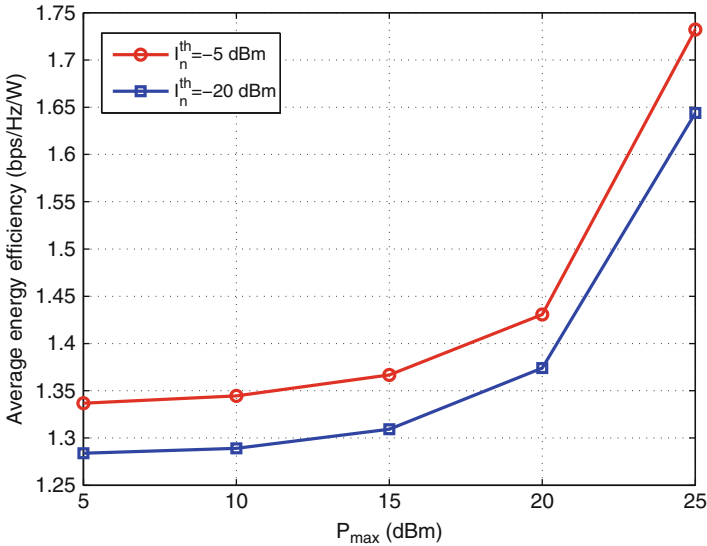


Fig. 10 Average energy efficiency versus P_{\max} with different cross-tier interference limits

interference limit $I_n^{\text{th}} = -20, -5$ dBm and target detection probability $\hat{q}_n^d = 0.9$ [19]. Similar to Fig. 4, Fig. 10 shows that the average energy efficiency of each subchannel in cognitive small cell increases when P_{\max} is increased from 5 to 25 dBm. Besides, the larger cross-tier interference limit can result in improved performance in average energy efficiency.

Figure 11 shows the convergence performance of Algorithm 1 in the network consists of multiple cognitive small cells under the different circuit power P_c . As shown in Fig. 11, the total average energy efficiency on each subchannel of all small cells converges after 12 iterations. The practical applicability of Algorithm 1 in the multiple cognitive small cells is demonstrated through this figure.

Figure 12 shows that the total average energy efficiency on each subchannel of all small cells versus the number of small cells in network with the co-tier interference limits $\gamma^{\text{th}} = -10, -20$ dBm, and $P_{\max} = 15$ dBm. As shown in Fig. 12, the total average energy efficiency on each subchannel of all small cells increase gradually with the number of small cells. However, the rate of increase is diminishing, and it is caused by the co-tier interference among small cells [19]. A larger co-tier interference limit which results in better performance of the optimal total average energy efficiency can be seen. It implies that the provided method not only can optimize the energy efficiency but also can mitigate the co-tier interference in multiple cognitive small cells.

Figure 13 shows the total average energy efficiency on each subchannel of all the small cells versus the number of small cells in network with the cross-tier interference limits $I_n^{\text{th}} = -10, -13$ dBm, and $P_{\max} = 15$ dBm. The total average energy efficiency on each subchannel increases and then drops when the number of

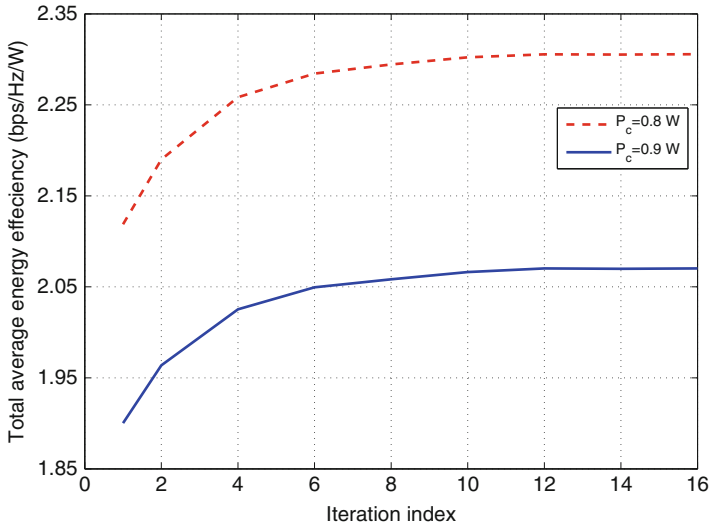


Fig. 11 Convergence in terms of sum of the average energy efficiency of small cells versus the number of iterations

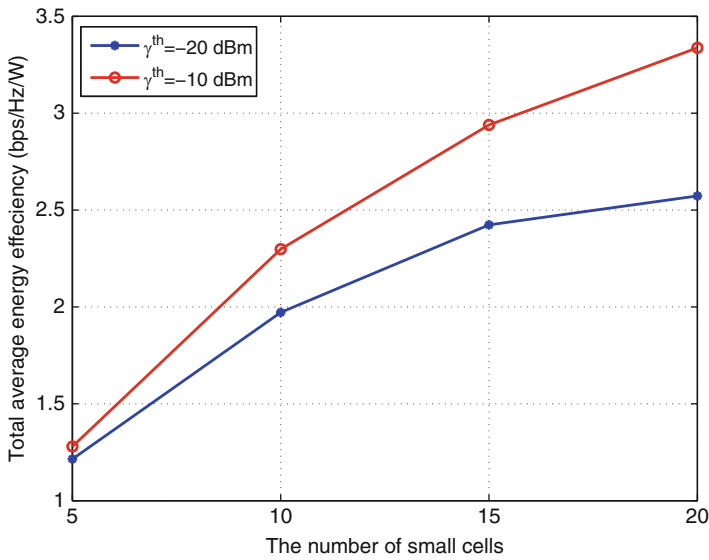


Fig. 12 Sum of the average energy efficiency versus the number of small cells with different co-tier interference limits

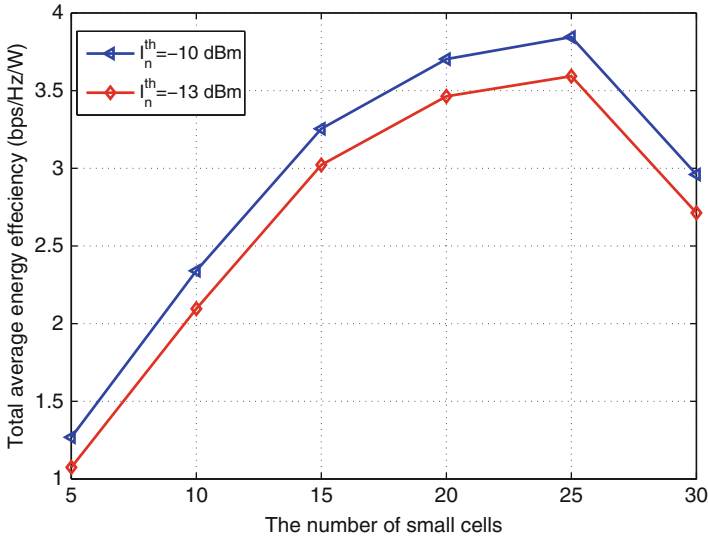


Fig. 13 Sum of the average energy efficiency versus the number of small cells with different cross-tier interference limits

small cells is increased from 5 to 30. The slope of lines is diminishing. Therefore, the provided scheme can mitigate the cross-tier interference when optimizing the energy efficiency.

Interference-Limited Resource Optimization in Cognitive Femtocells with Fairness and Imperfect Spectrum Sensing

This part studies joint subchannel and power allocation in OFDMA-based cognitive femtocells under femtocell user (FU) fairness constraints, QoS requirement, and co-/cross-tier interference temperature limits with imperfect spectrum sensing.

System Model

In the system model [18], we consider an OFDMA uplink of a network with one primary macrocell and K co-channel cognitive femtocells which are deployed randomly in the coverage area of a macrocell. Let M and F denote the numbers of active macro users (MUs) inside the primary macrocell and FUs in each cognitive femtocell, respectively. The OFDMA system has a bandwidth of B_w , which is divided into N_{total} subchannels. The channel model for each subchannel includes path loss and frequency-nonselective Rayleigh fading [18]. We focus on a resource allocation problem in the uplink of cognitive femtocells. The FUs opportunistically access the spectrum licensed to the primary macrocells via cognitive FBS, as illustrated in Fig. 14 [18]. In each time slot, the secondary network can sense N_{total}

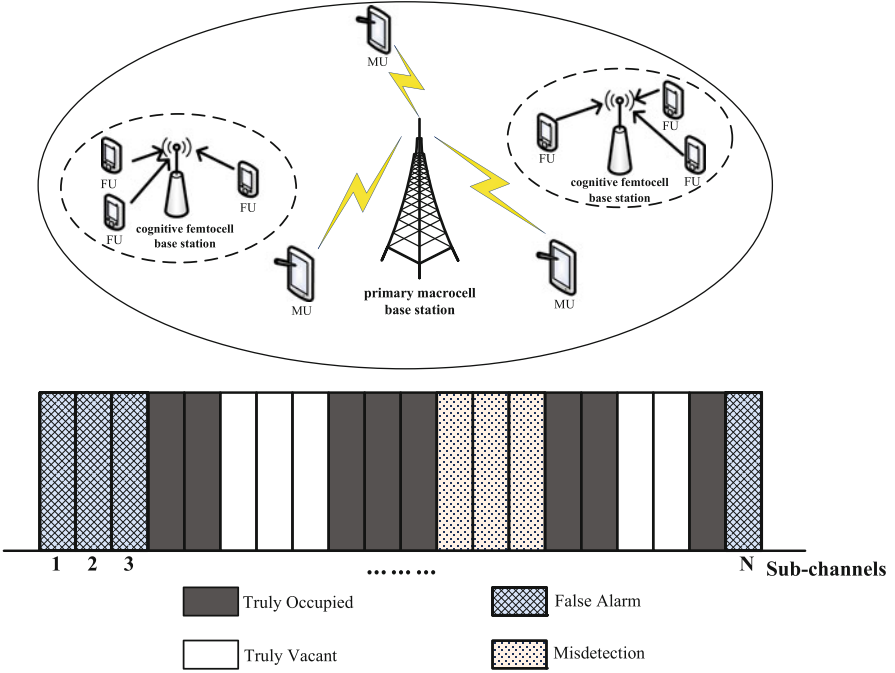


Fig. 14 A cognitive heterogeneous macro/femto network model

subchannels and opportunistically access idle channels by energy detection-based spectrum sensing. In a spectrum sensing period, the cognitive femtocell network senses N_{total} subchannels licensed to the primary macrocell network and determines available vacant/idle subchannels, which are denoted as $\mathcal{N} = 1, 2, \dots, N$. Throughout this part, a cognitive femto base station is assumed to have perfect channel state information (CSI) between FBS and cognitive FUs/primary MUs. Therefore, the total capacity of the cognitive femtocell networks using resource scheduling schemes [18] will serve as an upper bound of the achievable capacity with channel estimation errors in practical scenarios.

The received signal-to-interference-plus-noise ratio (SINR) $\ell_{k,i,n}^F$ at the k th ($k \in \{1, \dots, K\}$) cognitive FBS from its FU i ($i \in \{1, \dots, F\}$) in the n th ($n \in \{1, \dots, N\}$) subchannel is given as [18]

$$\ell_{k,i,n}^F = \frac{p_{k,i,n}^F \hat{h}_{k,k,i,n}^{FF}}{\sum_{j=1, j \neq k}^K \sum_{v=1}^F p_{j,v,n}^F \hat{h}_{k,j,v,n}^{FF} + p_{w,n}^M \hat{h}_{k,w,n}^{FM} + \sigma^2} \tag{47}$$

where $p_{k,i,n}^F$ is FU i 's transmit power on subchannel n in cognitive femtocell k ; $\hat{h}_{k,j,v,n}^{FF}$ and $\hat{h}_{k,w,n}^{FM}$ are the channel gains on subchannel n from FU v in cognitive femtocell j and from MU w to FBS k , respectively; w is a specific MU using

subchannel n ; $p_{w,n}^M$ is MU w 's transmit power in subchannel n ; and σ^2 is the additive white Gaussian noise (AWGN) power [18]. In such a case, based on the Shannon's capacity formula, the uplink capacity on subchannel n of FU i in cognitive femtocell k can be calculated by [18]

$$R_{k,i,n}^F = \log_2(1 + \ell_{k,i,n}^F). \quad (48)$$

Optimization Framework with Imperfect Spectrum Sensing

Imperfect Spectrum Sensing

Spectrum sensing has been extensively investigated in the previous works [24, 25]. Here, a cooperative spectrum sensing scheme [26] is presented, in which each cognitive FU senses subchannels and sends the sensing results to a cognitive FBS. Then, the cognitive FBS makes decision to determine whether or not the subchannels are vacant.

The interference from cognitive femtocell networks to primary macrocell networks occurs due to the following two reasons. One is the out-of-band emissions and the other is the spectrum sensing errors. The out-of-band emissions are due to power leakage in the sidelobes of OFDM signals [27]. The amount of out-of-band interference power of subchannel n introduced to subchannel j occupied by a primary macrocell (with unit transmit power) can be expressed as [18]

$$I_{k,i,n}^s = \int_{f_s^c - \frac{B_w}{2N_{\text{total}}} + f_n^c}^{f_s^c + \frac{B_w}{2N_{\text{total}}} + f_n^c} \varphi(f) \mathfrak{h}_{k,i,n,s}^{FM} df \quad (49)$$

where f_n^c and f_s^c are the center frequencies of subchannel n and s , respectively, and $\mathfrak{h}_{k,i,n,s}^{FM}$ is the channel gain from cognitive FU to primary MBS in subchannel s . In (47), power spectrum density (PSD) of OFDM signal $\varphi(f)$ is given as [18]

$$\varphi(f) = \frac{1}{T} \left(\frac{\sin(\pi(f - f_n^c)T)}{\pi(f - f_n^c)} \right)^2 \quad (50)$$

where T is the duration of an OFDM symbol.

Based on the analysis of the last part, there are four different cases in the cognitive femtocells network. Similarly, the probabilities for Cases 1, 2, 3, and 4 [18] for subchannel s are defined $\rho_{1,s}$, $\rho_{2,s}$, $\rho_{3,s}$, and $\rho_{4,s}$, respectively.

Based on the above analysis, the uplink cross-tier interference from cognitive femtocell to primary MBS, caused by out-of-band emission and co-channel interference, can be formulated as [18]

$$I_{k,i,n}^{MF} = p_{k,i,n}^F \underbrace{\left(\sum_{s \in \mathcal{N}_v} \rho_{3,s} I_{k,i,n}^s + \sum_{s \in \mathcal{N}_o} \rho_{4,s} I_{k,i,n}^s \right)}_{\tilde{G}_{k,i,n}^{MF}} \quad (51)$$

where \mathcal{N}_v and \mathcal{N}_o are the sets of vacant and occupied subchannels, respectively, and they are determined by the cognitive FBS. The amount of out-of-band interference power of subchannel n introduced to a primary macrocell-occupied subchannel j , with unit transmit power, can be expressed as $I_{k,i,n}^s$. In other words, since $I_{k,i,n}^s$ is calculated by unit transmit power, $I_{k,i,n}^s$ is the unit interference power here, which can be seen as channel gain. Moreover, both $\rho_{3,s}$ and $\rho_{4,s}$ are the probabilities, and therefore $\tilde{G}_{k,i,n}^{MF}$ can be interpreted as the channel gain on subchannel n from user i in cognitive femtocell k to the primary MBS [18].

General Optimization Framework

First, for resource allocation in cognitive femtocell networks, the total transmit power of cognitive FU is constrained by

$$\sum_{n=1}^N \tau_{k,i,n} P_{k,i,n}^F \leq P_{\max}, \quad \forall k, i \quad (52)$$

where $\tau_{k,i,n} \in \{0, 1\}$ is the subchannel allocation indicator, and $\tau_{k,i,n} = 1$ indicates that subchannel n is occupied by user i in cognitive femtocell k ; otherwise $\tau_{k,i,n} = 0$. P_{\max} is the maximum transmit power of each cognitive FU [18].

Second, to maintain communication quality of cognitive FUs, a QoS requirement in terms of SINR is introduced for each FU. Thus, the QoS requirement can be written as [18]

$$\sum_{n=1}^N \tau_{k,i,n} R_{k,i,n}^F \geq R_{k,i}^0, \quad \forall k, i \quad (53)$$

where $R_{k,i}^0$ is the QoS requirement for user i in cognitive femtocell k .

Third, a subchannel should be assigned to no more than one user at a time in a cognitive femtocell. Therefore, the subchannel assignment can be performed based on [18]

$$\sum_{i=1}^F \tau_{k,i,n} \leq 1, \quad \forall k, n. \quad (54)$$

Fourth, to obtain the fairness on FUs' level, the upper and lower bounds of the number of subchannels assigned to user i in cognitive femtocell k are set as [18]

$$\Gamma_{L,k,i} \leq \sum_{n=1}^N \tau_{k,i,n} \leq \Gamma_{U,k,i}, \quad \forall k, i \quad (55)$$

where $\Gamma_{U,k,i}$ and $\Gamma_{L,k,i}$ are the upper and lower bounds of the number of subchannels assigned to user i in cognitive femtocell k , respectively. Finally, to protect the primary macrocell's transmission, an interference temperature limit is introduced to constrain cross-tier interference from cognitive femtocell to primary macrocell [18], i.e.,

$$\sum_{k=1}^K \sum_{i=1}^F \tau_{k,i,n} p_{k,i,n}^F \tilde{G}_{k,i,n}^{MF} \leq I_{th,n}^{MF}, \quad \forall n \quad (56)$$

where $I_{th,n}^{MF}$ is the maximum tolerable cross-tier interference temperature in subchannel n in the primary macrocell.

Our resource allocation problem aims to maximize the total uplink capacity of K cognitive femtocells under a cross-tier interference constraint and FUs' QoS constraints, i.e. [18],

$$\begin{aligned} & \max_{\{\tau_{k,i,n}\}, \{p_{k,i,n}^F\}} \sum_{k=1}^K \sum_{i=1}^F \sum_{n=1}^N \tau_{k,i,n} R_{k,i,n}^F \quad (57) \\ \text{s.t. } & C_1 : \sum_{n=1}^N \tau_{k,i,n} p_{k,i,n}^F \leq P_{\max}, \quad \forall k, i, \\ & C_2 : p_{k,i,n}^F \geq 0, \quad \forall k, i, n, \\ & C_3 : \sum_{n=1}^N \tau_{k,i,n} R_{k,i,n}^F \geq R_{k,i}^0, \quad \forall k, i, \\ & C_4 : \tau_{k,i,n} \in \{0, 1\}, \quad \forall k, i, n, \\ & C_5 : \sum_{i=1}^F \tau_{k,i,n} \leq 1, \quad \forall k, n, \\ & C_6 : \Gamma_{L,k,i} \leq \sum_{n=1}^N \tau_{k,i,n} \leq \Gamma_{U,k,i}, \quad \forall k, i, \\ & C_7 : \sum_{k=1}^K \sum_{i=1}^F \tau_{k,i,n} p_{k,i,n}^F \tilde{G}_{k,i,n}^{MF} \leq I_{th,n}^{MF}, \quad \forall n \end{aligned}$$

where C_1 limits the transmit power of each FU below the maximum power P_{\max} ; C_2 indicates that the transmit power is nonnegative; C_3 sets the QoS requirement $R_{k,i}^0$ for user i in cognitive femtocell k ; C_4 and C_5 guarantee that each subchannel can be assigned to no more than one user in each femtocell; C_6 ensures a fairness among users by setting $\Gamma_{U,k,i}$ and $\Gamma_{L,k,i}$ as the upper and lower bounds of the number of subchannels assigned to user i in cognitive femtocell k , respectively. The priority of the user can be adjusted by setting appropriate values of $\Gamma_{U,k,i}$ and $\Gamma_{L,k,i}$. The constraint C_7 imposes the maximum tolerable cross-tier interference temperature $I_{th,n}^{MF}$ in subchannel n for the primary macrocell [18].

Joint Resource Optimization with Fairness and Imperfect Sensing

Transformation of the Optimization Problem

The problem in (57) is a non-convex mixed integer programming problem. It can be solved using a brute-force method, which however incurs a high computational complexity. To make the problem tractable, an additional co-tier interference temperature constraint C_8 is introduced as [18]

$$C_8 : \sum_{j=1, j \neq k}^K \sum_{v=1}^F \tau_{j,v,n} p_{j,v,n}^F \hat{h}_{k,j,v,n}^{\text{FF}} \leq I_{th,n}^{\text{FF}}, \quad \forall k, n \quad (58)$$

where $I_{th,n}^{\text{FF}}$ is the co-tier interference limit in subchannel n for a cognitive femtocell. Each femtocell will potentially interfere each other when two neighbor femtocells use the same subchannel. Therefore, from physical/engineering point view in the real-world applications, $I_{th,n}^{\text{FF}}$ is a co-tier interference limit for neighbor femtocell to mitigate co-tier interference. The value of $I_{th,n}^{\text{FF}}$ can be broadcasted by each femtocell or set by each femtocell.

Moreover, inspired by [28], the $\tau_{k,i,n}$ in C_4 is relaxed to be a real variable in the range of $[0,1]$, in which case $\tau_{k,i,n}$ can be interpreted as the fraction of time that subchannel n is assigned to user i in cognitive femtocell k during one transmission frame. Denote $\hat{p}_{k,i,n} = \tau_{k,i,n} p_{k,i,n}^F$ as the actual power allocated to user i in cognitive femtocell k on subchannel n . Denote $I_{k,i,n} = p_{w,n}^M \hat{h}_{k,w,n}^{\text{FM}} + I_{th,n}^{\text{FF}} + \sigma^2$ and $\hat{R}_{k,i,n}^F = \log_2 \left(1 + \frac{\hat{p}_{k,i,n} \hat{h}_{k,k,i,n}^{\text{FF}}}{\tau_{k,i,n} I_{k,i,n}} \right)$ as the upper bound of the total received interference power and lower bound of the capacity of user i on subchannel n in cognitive femtocell k , respectively. In such a case, the optimization problem in (57) can be rewritten as [18]

$$\begin{aligned} & \max_{\{\tau_{k,i,n}\}, \{\hat{p}_{k,i,n}\}} \sum_{k=1}^K \sum_{i=1}^F \sum_{n=1}^N \tau_{k,i,n} \hat{R}_{k,i,n}^F \quad (59) \\ \text{s.t. } & C_1 : \sum_{n=1}^N \hat{p}_{k,i,n} \leq P_{\max}, \quad \forall k, i, \\ & C_2 : \hat{p}_{k,i,n} \geq 0, \quad \forall k, i, n, \\ & C_3 : \sum_{n=1}^N \tau_{k,i,n} \hat{R}_{k,i,n}^F \geq R_{k,i}^0, \quad \forall k, i, \\ & C_4 : 0 \leq \tau_{k,i,n} \leq 1, \quad \forall k, i, n, \\ & C_5 : \sum_{i=1}^F \tau_{k,i,n} \leq 1, \quad \forall k, n, \end{aligned}$$

$$\begin{aligned}
C_6 : \Gamma_{L,k,i} &\leq \sum_{n=1}^N \tau_{k,i,n} \leq \Gamma_{U,k,i}, \quad \forall k, i, \\
C_7 : \sum_{k=1}^K \sum_{i=1}^F \widehat{p}_{k,i,n} \widetilde{G}_{k,i,n}^{\text{MF}} &\leq I_{th,n}^{\text{MF}}, \quad \forall n, \\
C_8 : \sum_{j=1, j \neq k}^K \sum_{v=1}^F \tau_{j,v,n} \widehat{h}_{k,j,v,n}^{\text{FF}} &\leq I_{th,n}^{\text{FF}}, \quad \forall k, n.
\end{aligned}$$

Theorem 2. *The objective function in (59) is concave, and the corresponding optimization problem under the constraints C_1 to C_8 is a convex problem.*

The proof is provided in Appendix.

According to Theorem 2, the objective function in (59) is concave, and the corresponding optimization problem under the constraints C_1 to C_8 is a convex problem.

Joint Subchannel and Power Allocation with Imperfect Spectrum Sensing

The joint subchannel and power allocation problem in (59) can be solved using the Lagrangian dual decomposition method, which has been widely used in solving resource allocation problems. The Lagrangian function is given by [18]

$$\begin{aligned}
\mathcal{L}(\{\tau_{k,i,n}\}, \{\widehat{p}_{k,i,n}\}, \boldsymbol{\lambda}, \mathbf{v}, \boldsymbol{\delta}, \boldsymbol{\mu}, \boldsymbol{\eta}) &= \sum_{k=1}^K \sum_{u=1}^F \sum_{n=1}^N \tau_{k,i,n} \widehat{R}_{k,i,n}^{\text{F}} \\
&+ \sum_{k=1}^K \sum_{i=1}^F \lambda_{k,i} \left(P_{\max} - \sum_{n=1}^N \widehat{p}_{k,i,n} \right) + \sum_{n=1}^N \delta_n \left(I_{th,n}^{\text{MF}} - \sum_{k=1}^K \sum_{i=1}^F \widehat{p}_{k,i,n} \widetilde{G}_{k,i,n}^{\text{MF}} \right) \\
&+ \sum_{k=1}^K \sum_{n=1}^N \mu_{k,n} \left(I_{th,n}^{\text{FF}} - \sum_{j=1, j \neq k}^K \sum_{v=1}^F \widehat{p}_{j,v,n} \widehat{h}_{k,j,v,n}^{\text{FF}} \right) + \sum_{k=1}^K \sum_{n=1}^N \eta_{k,n} \left(1 - \sum_{i=1}^F \tau_{k,i,n} \right) \\
&+ \sum_{k=1}^K \sum_{i=1}^F v_{k,i} \left(\sum_{n=1}^N \tau_{k,i,n} \widehat{R}_{k,i,n}^{\text{F}} - R_{k,i}^0 \right) \tag{60}
\end{aligned}$$

where $\boldsymbol{\lambda}$, \mathbf{v} , $\boldsymbol{\delta}$, $\boldsymbol{\mu}$, and $\boldsymbol{\eta}$ are the Lagrange multiplier vectors for C_1 , C_3 , C_7 , C_8 , and C_5 in (59), respectively. The boundary constraints C_2 , C_4 , and C_6 in (59) are absorbed in the KKT conditions [23], which will be shown later. The dual function is defined as

$$g(\boldsymbol{\lambda}, \mathbf{v}, \boldsymbol{\delta}, \boldsymbol{\mu}, \boldsymbol{\eta}) = \max_{\{\tau_{k,i,n}\}, \{\widehat{p}_{k,i,n}\}} \mathcal{L}(\{\tau_{k,i,n}\}, \{\widehat{p}_{k,i,n}\}, \boldsymbol{\lambda}, \mathbf{v}, \boldsymbol{\delta}, \boldsymbol{\mu}, \boldsymbol{\eta}) \tag{61}$$

and the dual problem can be expressed by

$$\min_{\lambda, \nu, \delta, \mu, \eta \geq 0} g(\lambda, \nu, \delta, \mu, \eta). \tag{62}$$

Decomposing the Lagrangian dual problem into a master problem and $K \times N$ subproblems that can be solved iteratively [18]. Here the MBS solves the master problem, and each FBS solves N subproblems based on local information in each iteration. Accordingly, Eq. (60) is rewritten as [18]

$$\begin{aligned} \mathcal{L}(\{\tau_{k,i,n}\}, \{\hat{p}_{k,i,n}\}, \lambda, \nu, \delta, \mu, \eta) &= \sum_{k=1}^K \sum_{n=1}^N L_{k,n}(\{\tau_{k,i,n}\}, \{\hat{p}_{k,i,n}\}, \lambda, \nu, \delta, \mu, \eta) \\ &+ \sum_{k=1}^K \sum_{i=1}^F \lambda_{k,i} P_{\max} - \sum_{k=1}^K \sum_{i=1}^F \nu_{k,i} R_{k,i}^0 + \sum_{n=1}^N \delta_n I_{th,n}^{MF} + \sum_{k=1}^K \sum_{n=1}^N \mu_{k,n} I_{th,n}^{FF} + \sum_{k=1}^K \sum_{n=1}^N \eta_{k,n} \end{aligned} \tag{63}$$

where

$$\begin{aligned} \mathcal{L}_{k,n}(\{\tau_{k,i,n}\}, \{\hat{p}_{k,i,n}\}, \lambda, \nu, \delta, \mu, \eta) &= \sum_{i=1}^F \tau_{k,i,n} \hat{R}_{k,i,n}^F - \sum_{i=1}^F \lambda_{k,i} \hat{p}_{k,i,n} - \sum_{i=1}^F \eta_{k,n} \tau_{k,i,n} \\ &+ \sum_{i=1}^F \nu_{k,i} \tau_{k,i,n} \hat{R}_{k,i,n}^F - \mu_{k,n} \sum_{j=1, j \neq k}^K \sum_{l \in U_j} \hat{p}_{j,l,n} \hat{h}_{k,j,l,n}^{FF} - \sum_{g \neq k}^K \sum_{u \in U_k} \mu_{g,n} \hat{p}_{k,i,n} \hat{h}_{g,k,i,n}^{FF} \\ &- \sum_{i=1}^F \delta_n \hat{p}_{k,i,n} \tilde{G}_{k,i,n}^{MF}. \end{aligned} \tag{64}$$

The calculation of the derivatives with respect to $\hat{p}_{k,i,n}$ and $\tau_{k,i,n}$, respectively, gives the KKT condition as

$$\frac{\partial L_{k,n}(\dots)}{\partial \hat{p}_{k,i,n}} = \Lambda_{k,i,n} - \lambda_{k,i} \leq 0 \tag{65}$$

where

$$\Lambda_{k,i,n} = \frac{(1 + \nu_{k,i}) \tau_{k,i,n} \hat{h}_{k,k,i,n}^{FF}}{\ln 2 (\tau_{k,i,n} I_{k,i,n} + \hat{p}_{k,i,n} \hat{h}_{k,k,i,n}^{FF})} - \sum_{g=1, g \neq k}^K \mu_{g,n} \hat{h}_{g,k,i,n}^{FF} - \delta_n \tilde{G}_{k,i,n}^{MF}, \tag{66}$$

$$\hat{p}_{k,i,n} (\Lambda_{k,i,n} - \lambda_{k,i}) = 0, \tag{67}$$

$$\lambda_{k,i} \left(P_{\max} - \sum_{n=1}^N \hat{p}_{k,i,n} \right) = 0. \tag{68}$$

According to (65), (66), (67), and (68), the optimal power allocated to user i in cognitive femtocell k in subchannel n for (59) is [18]

$$p_{k,i,n}^{*F} = \frac{\hat{p}_{k,i,n}}{\tau_{k,i,n}} = \left[\frac{(1 + \nu_{k,i})}{\ln 2 \left(\lambda_{k,i} + \sum_{g=1, g \neq k}^K \mu_{g,n} \hat{h}_{g,k,i,n}^{FF} + \delta_n \tilde{G}_{k,i,n}^{MF} \right)} - \frac{I_{k,i,n}}{\hat{h}_{k,k,i,n}^{FF}} \right]^+, \forall k, i \quad (69)$$

where $[x]^+ = \max\{0, x\}$. Moreover, there is

$$\frac{\partial L_{k,n}(\dots)}{\partial \tau_{k,i,n}} = \mathcal{E}_{k,i,n} - \eta_{k,n} \leq 0 \quad (70)$$

where

$$\mathcal{E}_{k,i,n} = (1 + \nu_{k,i}) \left[\log_2 \left(1 + \frac{p_{k,i,n}^{*F} \hat{h}_{k,k,i,n}^{FF}}{I_{k,i,n}} \right) - \frac{1}{\ln 2} \left(\frac{p_{k,i,n}^{*F} \hat{h}_{k,k,i,n}^{FF}}{p_{k,i,n}^{*F} \hat{h}_{k,k,i,n}^{FF} + I_{k,i,n}} \right) \right], \quad (71)$$

$$\tau_{k,i,n} (\mathcal{E}_{k,i,n} - \eta_{k,n}) = 0, \quad (72)$$

$$\eta_{k,n} \left(1 - \sum_{i=1}^F \tau_{k,i,n} \right) = 0. \quad (73)$$

Based on (70), (71), (72), and (73), subchannel n is assigned to the user with the largest $\mathcal{E}_{k,i,n}$ in femtocell k , i.e.,

$$\hat{\tau}_{k,i^*,n} = 1 \Big|_{i^* = \max_i \mathcal{E}_{k,i,n}}, \quad \forall k, n. \quad (74)$$

Since the dual function is differentiable, the subgradient method can be used to solve the master dual minimization problem in (62). Based on the subgradient method, the master dual problem in (62) can be solved as [18]

$$\lambda_{k,i}^{(l+1)} = \left[\lambda_{k,i}^{(l)} - \varepsilon_1^{(l)} \left(P_{\max} - \sum_{n=1}^N \hat{p}_{k,i,n} \right) \right]^+, \quad \forall k, i, \quad (75)$$

$$\nu_{k,i}^{(l+1)} = \left[\nu_{k,i}^{(l)} - \varepsilon_2^{(l)} \left(\sum_{n=1}^N \hat{R}_{k,i,n}^F - R_{k,i}^0 \right) \right]^+, \quad \forall k, i, \quad (76)$$

$$\mu_{k,n}^{(l+1)} = \left[\mu_{k,n}^{(l)} - \varepsilon_3^{(l)} \left(I_{th,n}^{FF} - \sum_{j \neq k} \sum_{l \in U_j} s_{j,l,n} \hat{h}_{k,j,l,n}^{FF} \right) \right]^+, \quad \forall k, n, \quad (77)$$

$$\delta_n^{(l+1)} = \left[\delta_n^{(l)} - \varepsilon_4^{(l)} \left(I_{th,n}^{MF} - \sum_{k=1}^K \sum_{i=1}^F \hat{p}_{k,i,n} \tilde{G}_{k,i,n}^{MF} \right) \right]^+, \quad \forall n \quad (78)$$

where $\varepsilon_1^{(l)}$, $\varepsilon_2^{(l)}$, $\varepsilon_3^{(l)}$, and $\varepsilon_4^{(l)}$ are step sizes of iteration i , $l \in \{1, 2, \dots, L_{\max}\}$, L_{\max} is the maximal number of iterations. The step sizes should satisfy $\sum_{l=1}^{\infty} \varepsilon_t^{(l)} = \infty$, $\lim_{l \rightarrow \infty} \varepsilon_t^{(l)} = 0, \forall t \in 1, \dots, 4$. λ , ν , and μ are updated by the cognitive femtocells in a distributed manner, and $\delta_n^{(l+1)}$ is updated by the primary MBS. Figure 15 shows the three-layer architecture of the decomposed dual problem.

Iterative Resource Optimization Algorithm with Fairness

Although in the solution in (69), (74), (75), (76), (77), and (78) give a complete algorithm for the original problem, the fairness in subchannel occupation was not considered. Therefore, Algorithm 3 is provided as an implementation of the joint subchannel and power allocation scheme, as shown in the pseudo codes below.

In this part, the fairness is taken into consideration in terms of subchannel allocation. Specifically, to ensure the fairness on FUs' level, the upper and lower bounds of the number of subchannels are assigned to the users in a cognitive femtocell as shown in (55). In the problem formulation, C_6 ensures fairness among users by setting $\Gamma_{U,k,i}$ and $\Gamma_{L,k,i}$ as the upper and lower bounds of the number of

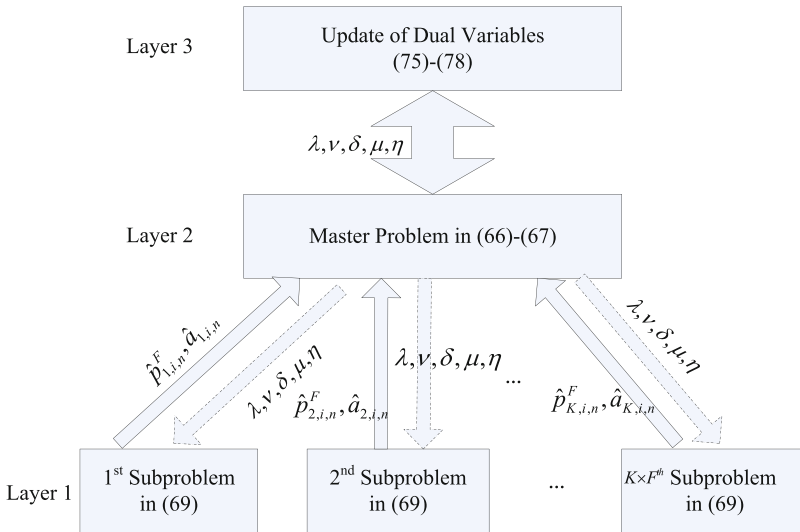


Fig. 15 Three-layer architecture of the decomposed dual problem

Algorithm 3 Iterative resource allocation algorithm

```

1: Cognitive FBS set:  $\mathcal{K} = \{1, 2, \dots, K\}$ ; Cognitive FU set per femtocell:  $\mathcal{U} = \{1, 2, \dots, F\}$ .
2: Initialize  $I_{\max}$  and Lagrangian variables vectors  $\lambda, \nu, \mu$ , and set  $i = 0$ .
3: Allocate the same power to each subchannel, set  $\tau_{k,i,n} = 0, \forall k, i, n$ .
4: repeat
5:   Cognitive FBS  $k$  measures  $\hat{h}_{k,k,i,n}^{\text{FF}}$  and  $I_{k,i,n}, \forall k, i, n$ ;
6:   for each FBS do
7:     subchannel set:  $\mathcal{N} = \{1, 2, \dots, N\}$ ;
8:     Set  $N_i = 0, \forall i \in \mathcal{U}$ 
9:     subchannel allocation for user fairness
10:    while  $N_i < \Gamma_{L,k,i}, \forall i \in \mathcal{U}$  do
11:      a) find  $n^* = \arg \max_{n \in \mathcal{N}} \mathcal{E}_{k,i,n}$  according to (71);
12:      b)  $\tau_{k,i,n^*} = 1, \mathcal{N} = \mathcal{N} - \{n^*\}, N_i = N_i + 1$ ;
13:      if  $N_i = N_{U,k,i}$  then
14:         $\mathcal{U} = \mathcal{U} - \{i\}$ ;
15:      end if
16:    end while
17:    subchannel allocation for capacity enhancement
18:    while  $\mathcal{N} \neq \phi$  do
19:      a) find  $(i^*, n^*) = \arg \max_{i \in \mathcal{U}, n \in \mathcal{N}} \mathcal{E}_{k,i,n}$ ;
20:      b)  $\tau_{k,i^*,n^*} = 1, \mathcal{N} = \mathcal{N} - \{n^*\}$ ;
21:      if  $N_{i^*} = N_{U,k,i^*}$  then
22:         $\mathcal{U} = \mathcal{U} - \{i^*\}$ ;
23:      end if
24:    end while
25:    Every FBS  $j (j \neq k)$  measures  $\mu_{j,n} \hat{h}_{j,k,i,n}^{\text{FF}}$  and feeds it back to FBS  $k$ 
26:    Power Allocation
27:    for  $n = 1$  to  $N$  do
28:      a) FUs update  $p_{k,i,n}^{*F}$  according to (69);
29:      b) Cognitive FBS  $k$  updates  $\lambda, \nu, \mu$  according to (75), (76) and (77), respectively;
30:      c) Cognitive FBS  $k$  updates  $\mathcal{E}_{k,i,n}$  according to (71).
31:    end for
32:    end for
33:    Primary MBS updates  $\delta$  according to (78), and broadcasts the updated value to all FBSs
    via backhaul,  $l = l + 1$ .
34: until convergence or  $l = L_{\max}$ 

```

subchannels assigned to user i in cognitive femtocell k , respectively, and the priority of the user can be adjusted by setting values of $\Gamma_{U,k,i}$ and $\Gamma_{L,k,i}$ appropriately. After the transformation, the optimization problem is solved by Algorithm 3 [18].

In Algorithm 3, there are two procedures to ensure users' fairness in subchannel allocation. First, subchannels are allocated for the users whose subchannel occupation is below $\Gamma_{L,k,i}$, and this procedure is named as "subchannel allocation for user fairness" in Algorithm 3, to guarantee user's lowest requirement. In the second procedure, which is called "subchannel allocation for capacity enhancement," the algorithm tries to enhance the user's capacity while keeping users' subchannel occupation below the upper bound of $\Gamma_{U,k,i}$. With the help of the two procedures, Algorithm 3 can ensure that the subchannels assigned to user i in femtocell k is

between $\Gamma_{U,k,i}$ and $\Gamma_{L,k,i}$. Moreover, from lines 9–16 of Algorithm 3, subchannels will be assigned to cognitive femto users, and the used subchannels will be removed from subchannel set \mathcal{N} based on line 12 of Algorithm 3. Algorithm 3 will check that whether any unused subchannels are left in line 18; if true, lines 19–20 will be executed until the subchannel set is empty. Therefore, lines 9–24 can ensure a full utilization of all vacant subchannels [18].

In practical scenarios, users' subchannel requirements are different, and traditional capacity-maximum subchannel algorithms tend to allocate the subchannels to the users with better channel conditions according to users' subchannel requirements. Therefore, the subchannel requirements of the other users with relatively poor channel conditions may not be satisfied. This is unfair for the users with poor subchannel conditions. In Algorithm 3, Procedure 1 can guarantee the lowest requirements of subchannels for users with poor channel conditions, and Procedure 2 can maximize the users' capacity while keeping the number of user's subchannel occupation below the upper bound.

Note that $h_{g,k,i,n}^{\text{FF}}$ required in (69), (71), and (77) can be known by a cognitive FBS from a FBS gateway or through available interfaces between FBSs, and $\tilde{G}_{k,i,n}^{\text{MF}}$ required in (69) and (78) can be estimated by user i in femtocell k by measuring downlink channel gain of subchannel n from the MBS, assuming a symmetry between uplink and downlink channels. Furthermore, it is assumed that there are wired connections between FBSs and MBS [29,30], so that $\tilde{G}_{k,i,n}^{\text{MF}}$ can be exchanged between the MBS and FBS's.

The following is the complexity analysis of the provided algorithm. Suppose that the subgradient method used in Algorithm 3 needs Δ iterations to converge. Since the updates of each λ and ν need $O(F)$ operations [23], the computation of μ and δ requires $O(N)$ operations each, and Δ is a polynomial function of FN . Therefore, the asymptotic complexity of Algorithm 3 is $O(KFN(\log_2 N + \log_2 F)\Delta)$. Compared to the brute-force method, which has a complexity of $O(KF^N)$, the provided Algorithm 3 has a lower complexity, especially for a large N .

Simulation Results and Discussions

In the simulations, the primary macrocell's radius is set to 500 m, and the radius of each cognitive femtocell is set to 10 m. Cognitive femtocells and MUs are distributed randomly in the macrocell coverage area. The carrier frequency is 2 GHz. $B_w = 10$ MHz, $N_0 = -174$ dBm/Hz, $N = 50$, and $M = 20$ were used in the simulations, respectively [18]. The block-fading channel gains are modeled as independent identically distributed exponential random variables with unit mean. MUs' maximum transmit power is 23 dBm. The standard deviation of lognormal shadowing between MBS and users is 8 dB, while between an FBS and users is 10 dB. The probability of false alarm q_s^f , mis-detection q_s^m , and primary MU's occupation q_s^p are uniformly distributed over [0.05,0.1], [0.01,0.05], and [0,1], respectively. Assuming that $\mathcal{N}_o = \{1, 3, 5, \dots, 49\}$ and $\mathcal{N}_v = \{2, 4, 6, \dots, 50\}$,

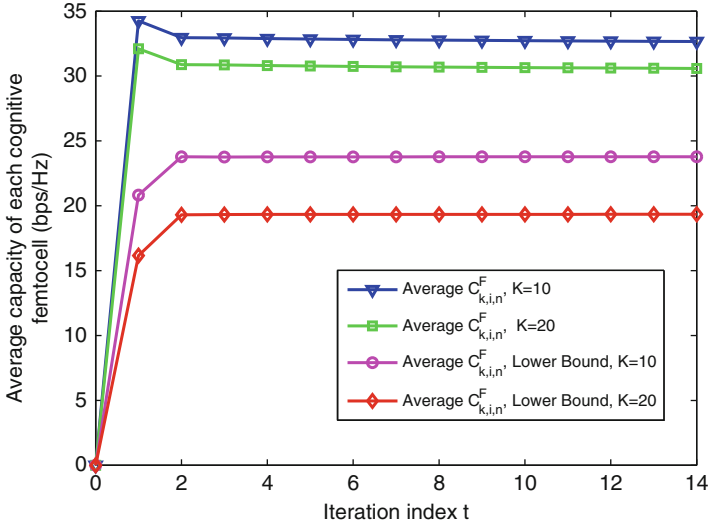


Fig. 16 Convergence in terms of average capacity of each femtocell versus the number of iterations

while the upper bounds [7, 7, 14, 14] and the lower bounds [3, 3, 7, 7] of subchannel assignment for FUs $i = \{1, 2, 3, 4\}$ per femtocell are assumed. For comparison purpose, the simulation included the scheduling scheme in [31] in conjunction with the power allocation scheme in Algorithm 3 and referred to it as the “existing scheme” hereafter. The indoor and outdoor pathloss models are based on [32].

Figure 16 shows the convergence of the Algorithm 3 in terms of the average capacity per femtocell versus the number of iterations i , where $K = 10, 20$, $R_{k,i}^0 = 9$ bps/Hz for all FUs, $P_{\max} = 23$ dBm, and $I_{th,n}^{FF} = I_{th,n}^{MF} = -100$ dBm. The provided algorithm in [18] takes only four iterations to converge, indicating that it is suitable for real-time implementation. The average capacity per femtocell for $K = 10$ is higher than that for $K = 20$, because co-tier interference increases with K . The lower bound of cognitive femtocell capacity used in (59) is also plotted and is shown to be in reasonably close agreement with the simulation results.

Figure 17 shows the total capacity of K cognitive femtocells versus the number of femtocells in term of different co-/cross-tier interference limits. The Algorithm 3 [18] with higher co-/cross-tier interference limits, $I_{th,n}^{FF}$ and $I_{th,n}^{MF}$, provides a higher total capacity of K cognitive femtocells, because of the higher transmit power used by users under the slacker constraint of co-/cross-tier interference. The effect on how additional constraint of C_8 affects the overall performance of the Algorithm 3 is investigated in the simulations, as showed in Fig. 17. The brute-force method without constraint of co-tier interference limit C_8 has a better performance in terms of total capacity of K cognitive femtocells than the provided algorithm with C_8 , because of the slacker constraint of co-/cross-tier interference in the optimization problem [18].

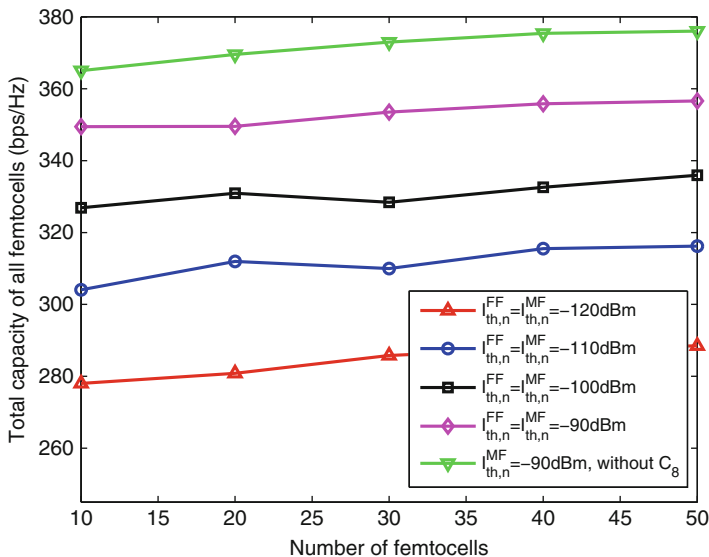


Fig. 17 Total capacity of femtocells versus number of femtocells

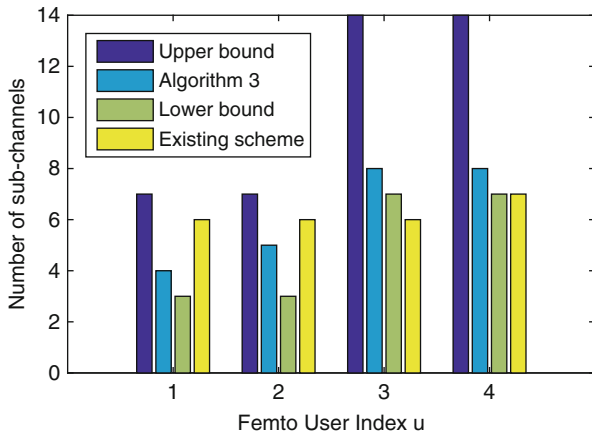


Fig. 18 Number of subchannels occupied by each FU

Figure 18 shows the average number of subchannels allocated by the provided Algorithm 3 [18] to each FU as compared with the “existing algorithm.” It can be seen that subchannel assignments of the provided algorithm meet the requirements of different users given in C_6 , while the “existing algorithm” does not always satisfy C_6 , e.g., the number of assigned subchannels may fall below the lower bound. The provided algorithm tends to allocate a number of subchannels, which

is only slightly larger than the lower bound to each FU, leading to an efficient reuse of subchannels. The procedure of “subchannel allocation for user fairness” guarantees the lower bound for users’ subchannel requirement, while the procedure of “subchannel allocation for capacity enhancement” guarantees that it does not exceed the upper bound.

Figure 19a shows the average cross-tier interference suffered in each subchannel of primary macrocell when the maximum transmit power P_{\max} increases from 20 to 30 dBm, for the number of users per femtocell $F = 4$ and the number of femtocells $K = 10$. The other simulation parameters are set as $R_{k,i}^0 = 9$ bps/Hz for all k , and $I_{th,n}^{MF} = I_{th,n}^{FF} = -100$ dBm for all n . The total cross-tier interference increases as the increase of P_{\max} . This is because that the cross-tier interference is caused by transmit power per subchannel and the cross-tier channel gain, and a large value of P_{\max} enlarges the feasible domain of the optimizing variable [18]. It also can be seen from the figure that the perfect spectrum sensing scheme has a higher cross-tier interference than the imperfect spectrum sensing scheme. The reason of this phenomenon is that mis-detection and false alarm in imperfect spectrum sensing overestimate the cross-tier interference. Moreover, the average interference from cognitive femtocell to primary macrocell in each sub-channel in imperfect spectrum sensing is below the cross-tier interference threshold. Figure 19b shows the average co-tier interference suffered in each subchannel of neighboring femtocells when maximum transmit power P_{\max} increases from 20 to 30 dBm. Note that perfect spectrum sensing of cross-tier channel gain at cognitive FBS side results in a higher co-tier interference than the imperfect spectrum sensing scheme [18], because mis-detection and false alarm in imperfect spectrum sensing overestimate the cross-tier interference.

Figure 20 shows the total capacity of all cognitive femtocells when maximum transmit power P_{\max} increases from 20 to 30 dBm, for the number of users per femtocell $F = 4$ and the number of femtocells $K = 10$. The other simulation parameters are set as $R_{k,i}^0 = 9$ bps/Hz for all k , and $I_{th,n}^{MF} = I_{th,n}^{FF} = -100$ dBm for all n . The total capacity of all femtocells increases with P_{\max} . This is because a large value of P_{\max} enlarges the feasible domain of the optimizing variable [18]. It also can be seen from the figure that perfect spectrum sensing scheme has a higher capacity of all cognitive femtocells than the imperfect spectrum sensing scheme, because mis-detection and false alarm in imperfect spectrum sensing overestimate the cross-tier interference, which shrinks the feasible domain of the optimizing variable.

Figure 21 shows the total capacity of all cognitive femtocells when minimum transmit rate requirement $R_{k,i}$ increases from 2 to 10 bps/Hz for the number of users per femtocell $F = 2, 3, 4$ and the number of femtocells $K = 10$. The other simulation parameters are set as $I_{th,n}^{MF} = I_{th,n}^{FF} = -100$ dBm for all n . The total capacity of all femtocells decreases as the decrease of $R_{k,i}^0$. This is because a large value of $R_{k,i}^0$ narrows the feasible domain of the optimizing variable. It can also be seen from the figure that a larger number of FUs per femtocell results in a higher capacity, because of the multiuser diversity in the resource allocation [18].

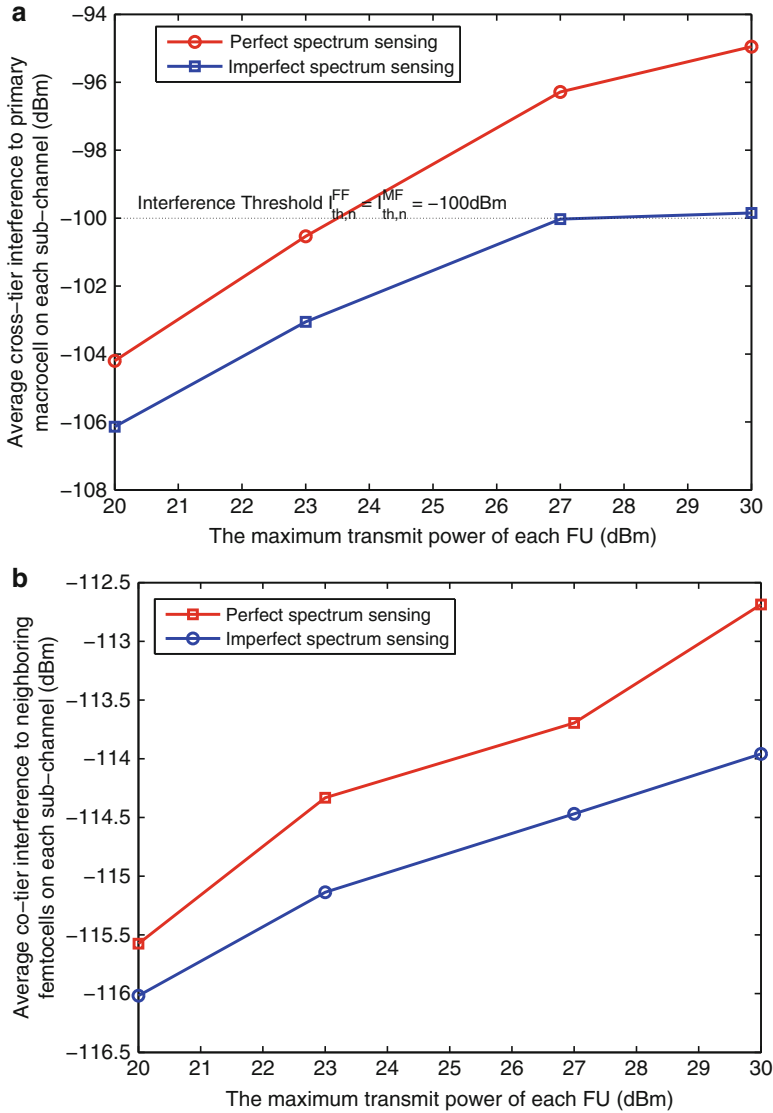


Fig. 19 Average cross-tier interference to primary macrocell and average co-tier interference to neighboring femtocells in each subchannel versus the maximum transmit power of each FU. **(a)** Average cross-tier interference to primary macrocell in each subchannel. **(b)** Average co-tier interference to neighboring femtocells in each subchannel

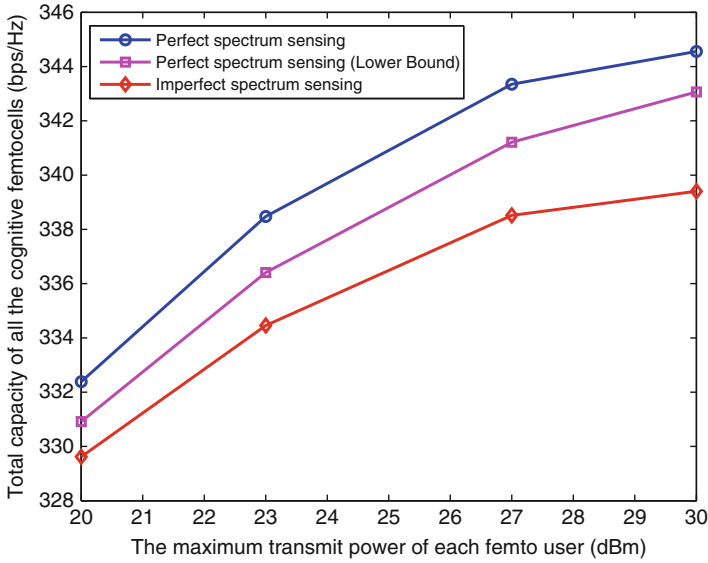


Fig. 20 Total capacity of all cognitive femtocells versus the maximum transmit power of each FU

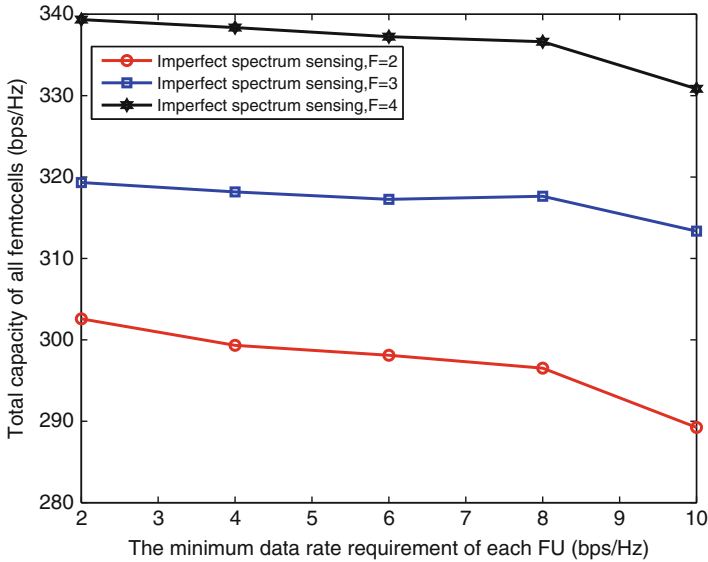


Fig. 21 Total capacity of all cognitive femtocells versus the minimum QoS requirement of each FU

Conclusion

This chapter introduced the resource allocation problem in cognitive heterogeneous networks, where the cross-tier interference mitigation, imperfect spectrum sensing, and energy efficiency are considered. Through provided three algorithms for cognitive heterogeneous networks, the resource allocation problems were solved. Furthermore, the simulation results showed that the provided algorithms achieve improved performance.

Appendix

The proof of Theorem 1.

Proof. (1) Suppose that $\eta_{13,n}^*$ is the optimal solution of (22), the inequality can be obtained

$$\begin{aligned} \eta_{13,n}^* &= \frac{P(\mathcal{H}_n^v)(1 - q_n^f(\varepsilon_n, \hat{\tau}))R_{1,n}(\hat{\tau}, \tilde{P}_{s,n}^v) + P(\mathcal{H}_n^o)q_n^m(\varepsilon_n, \hat{\tau})R_{3,n}(\hat{\tau}, \tilde{P}_{s,n}^v)}{\tilde{P}_{s,n}^v + P_c} \\ &\geq \frac{P(\mathcal{H}_n^v)(1 - q_n^f(\varepsilon_n, \hat{\tau}))R_{1,n}(\hat{\tau}, P_{s,n}^v) + P(\mathcal{H}_n^o)q_n^m(\varepsilon_n, \hat{\tau})R_{3,n}(\hat{\tau}, P_{s,n}^v)}{P_{s,n}^v + P_c} \end{aligned} \quad (79)$$

$$\begin{aligned} \max_{P_{s,n}^v} \left\{ P(\mathcal{H}_n^v)(1 - q_n^f(\varepsilon_n, \hat{\tau}))R_{1,n}(\hat{\tau}, P_{s,n}^v) + P(\mathcal{H}_n^o)q_n^m(\varepsilon_n, \hat{\tau})R_{3,n}(\hat{\tau}, P_{s,n}^v) - \eta_{13,n}^*(P_{s,n}^v + P_c) \right\} \\ = P(\mathcal{H}_n^v)(1 - q_n^f(\varepsilon_n, \hat{\tau}))R_{1,n}(\hat{\tau}, P_{s,n}^v) + P(\mathcal{H}_n^o)q_n^m(\varepsilon_n, \hat{\tau})R_{3,n}(\hat{\tau}, P_{s,n}^v) - \eta_{13,n}^*(P_{s,n}^v + P_c) = 0. \end{aligned} \quad (80)$$

Hence, we have (81)

$$\begin{cases} P(\mathcal{H}_n^v)(1 - q_n^f(\varepsilon_n, \hat{\tau}))R_{1,n}(\hat{\tau}, \tilde{P}_{s,n}^v) + P(\mathcal{H}_n^o)q_n^m(\varepsilon_n, \hat{\tau})R_{3,n}(\hat{\tau}, \tilde{P}_{s,n}^v) - \eta_{13,n}^*(\tilde{P}_{s,n}^v + P_c) = 0 \\ P(\mathcal{H}_n^v)(1 - q_n^f(\varepsilon_n, \hat{\tau}))R_{1,n}(\hat{\tau}, P_{s,n}^v) + P(\mathcal{H}_n^o)q_n^m(\varepsilon_n, \hat{\tau})R_{3,n}(\hat{\tau}, P_{s,n}^v) - \eta_{13,n}^*(P_{s,n}^v + P_c) \leq 0. \end{cases} \quad (81)$$

$$\text{Therefore, } \max_{P_{s,n}^v} \left\{ \begin{array}{l} P(\mathcal{H}_n^v)(1 - q_n^f(\varepsilon_n, \hat{\tau}))R_{1,n}(\hat{\tau}, P_{s,n}^v) \\ + P(\mathcal{H}_n^o)q_n^m(\varepsilon_n, \hat{\tau})R_{3,n}(\hat{\tau}, P_{s,n}^v) \\ - \eta_{13,n}^*(P_{s,n}^v + P_c) \end{array} \right\} = 0 \text{ can be concluded.}$$

That is, eq. (80) is achieved.

(2) Suppose that $\tilde{P}_{s,n}^v$ is a solution to the problem of (80). The definition of (80) implies that (82)

$$\begin{aligned}
& P(\mathcal{H}_n^v)(1 - q_n^f(\varepsilon_n, \hat{\tau}))R_{1,n}(\hat{\tau}, P_{s,n}^v) + P(\mathcal{H}_n^o)q_n^m(\varepsilon_n, \hat{\tau})R_{3,n}(\hat{\tau}, P_{s,n}^v) \\
& - \eta_{13,n}^*(P_{s,n}^v + P_c) \leq P(\mathcal{H}_n^v)(1 - q_n^f(\varepsilon_n, \hat{\tau}))R_{1,n}(\hat{\tau}, \tilde{P}_{s,n}^v) \\
& + P(\mathcal{H}_n^o)q_n^m(\varepsilon_n, \hat{\tau})R_{3,n}(\hat{\tau}, \tilde{P}_{s,n}^v) - \eta_{13,n}^*(\tilde{P}_{s,n}^v + P_c) = 0 \\
& \text{or} \\
& \begin{cases} P(\mathcal{H}_n^v)(1 - q_n^f(\varepsilon_n, \hat{\tau}))R_{1,n}(\hat{\tau}, P_{s,n}^v) + P(\mathcal{H}_n^o)q_n^m(\varepsilon_n, \hat{\tau})R_{3,n}(\hat{\tau}, P_{s,n}^v) \\ - \eta_{13,n}^*(P_{s,n}^v + P_c) \leq 0 \\ P(\mathcal{H}_n^v)(1 - q_n^f(\varepsilon_n, \hat{\tau}))R_{1,n}(\hat{\tau}, \tilde{P}_{s,n}^v) + P(\mathcal{H}_n^o)q_n^m(\varepsilon_n, \hat{\tau})R_{3,n}(\hat{\tau}, \tilde{P}_{s,n}^v) \\ - \eta_{13,n}^*(\tilde{P}_{s,n}^v + P_c) = 0. \end{cases} \quad (82)
\end{aligned}$$

Therefore, we obtain

$$\frac{\left\{ \begin{array}{l} P(\mathcal{H}_n^v)(1 - q_n^f(\varepsilon_n, \hat{\tau}))R_{1,n}(\hat{\tau}, \tilde{P}_{s,n}^v) \\ + P(\mathcal{H}_n^o)q_n^m(\varepsilon_n, \hat{\tau})R_{3,n}(\hat{\tau}, \tilde{P}_{s,n}^v) \end{array} \right\}}{\tilde{P}_{s,n}^v + P_c} = \eta_{13,n}^* \quad (83)$$

and

$$\frac{\left\{ \begin{array}{l} P(\mathcal{H}_n^v)(1 - q_n^f(\varepsilon_n, \hat{\tau}))R_{1,n}(\hat{\tau}, P_{s,n}^v) \\ + P(\mathcal{H}_n^o)q_n^m(\varepsilon_n, \hat{\tau})R_{3,n}(\hat{\tau}, P_{s,n}^v) \end{array} \right\}}{P_{s,n}^v + P_c} \leq \eta_{13,n}^*. \quad (84)$$

□

Lemma 1. Let \mathbf{A} be an $N \times N$ symmetric matrix, \mathbf{A} is negative semidefinite if and only if all the k th order principal minors of \mathbf{A} are no larger than zero if k is odd, and not less than zero if k is even, where $1 \leq k \leq N$.

The proof of Theorem 2.

Proof. First, define the element $\tau_{k,i,n} \hat{R}_{k,i,n}^F$ in (59) as $f(\tau_{k,i,n}, \hat{p}_{k,i,n}) = \tau_{k,i,n} \hat{R}_{k,i,n}^F$. The objective function in (59) is the sum of $f(\tau_{k,i,n}, \hat{p}_{k,i,n})$ over all possible values of k , i , and n . Substituting $\hat{R}_{k,i,n}^F = \log_2 \left(1 + \frac{\hat{p}_{k,i,n} \mathbf{h}_{k,k,i,n}^{\text{FF}}}{\tau_{k,i,n} I_{k,i,n}} \right)$ into $f(\tau_{k,i,n}, \hat{p}_{k,i,n})$, so we have

$$f(\tau_{k,i,n}, \hat{p}_{k,i,n}) = \tau_{k,i,n} \log_2 \left(1 + \frac{\hat{p}_{k,i,n} \mathbf{h}_{k,k,i,n}^{\text{FF}}}{\tau_{k,i,n} I_{k,i,n}} \right). \quad (85)$$

Based on (85), one obtains

$$\frac{\partial^2 f}{\partial \tau_{k,i,n}^2} = -\frac{1}{\ln 2} \frac{(\hat{p}_{k,i,n} \mathbf{h}_{k,k,i,n}^{\text{FF}})^2}{\tau_{k,i,n} (\tau_{k,i,n} I_{k,i,n} + \hat{p}_{k,i,n} \mathbf{h}_{k,k,i,n}^{\text{FF}})^2}, \quad (86)$$

$$\frac{\partial^2 f}{\partial \tau_{k,i,n} \partial \widehat{p}_{k,i,n}} = \frac{\partial^2 f}{\partial \widehat{p}_{k,i,n} \partial \tau_{k,i,n}} = \frac{1}{\ln 2} \frac{\widehat{p}_{k,i,n} (\hbar_{k,k,i,n}^{\text{FF}})^2}{(\tau_{k,i,n} I_{k,i,n} + \widehat{p}_{k,i,n} \hbar_{k,k,i,n}^{\text{FF}})^2}, \quad (87)$$

$$\frac{\partial^2 f}{\partial \widehat{p}_{k,i,n}^2} = -\frac{1}{\ln 2} \frac{\tau_{k,i,n} (\hbar_{k,k,i,n}^{\text{FF}})^2}{(\tau_{k,i,n} I_{k,i,n} + \widehat{p}_{k,i,n} \hbar_{k,k,i,n}^{\text{FF}})^2}. \quad (88)$$

Consequently, the Hessian matrix of $f(\tau_{k,i,n}, \widehat{p}_{k,i,n})$ can be written as

$$\mathbf{H} = \begin{bmatrix} \frac{\partial^2 f}{\partial \tau_{k,i,n}^2} & \frac{\partial^2 f}{\partial \tau_{k,i,n} \partial \widehat{p}_{k,i,n}} \\ \frac{\partial^2 f}{\partial \widehat{p}_{k,i,n} \partial \tau_{k,i,n}} & \frac{\partial^2 f}{\partial \widehat{p}_{k,i,n}^2} \end{bmatrix}. \quad (89)$$

Substituting (86), (87), (88) to (89), we can show that the first-order principal minors of \mathbf{H} are negative, and the second-order principal minor of \mathbf{H} is zero. Therefore, \mathbf{H} is negative semidefinite according to Lemma 1, and $f(\tau_{k,i,n}, \widehat{p}_{k,i,n})$ is concave. The objective function of (59) is concave because any positive linear combination of concave functions is concave [23, 33]. As the inequality constraints in (59) are convex, the feasible set of the objective function in (59) is convex, and the corresponding optimization problem is a convex problem. This completes the proof. \square

References

1. Zhang H, Chu X, Guo W, Wang S (2015) Coexistence of Wi-Fi and heterogeneous small cell networks sharing unlicensed spectrum. *IEEE Commun Mag* 22(3):92–99
2. Samarakoon S, Bennis M, Saad W, Debbah M, Latva-aho M (2016) Ultra dense small cell networks: turning density into energy efficiency. *IEEE J Sel Areas Commun* 34(5): 1267–1280
3. Zhang H, Dong Y, Cheng J, Hossain Md J, Leung VCM (2016) Fronthauling for 5G LTE-U ultra dense cloud small cell networks. *IEEE Wirel Commun* 23(6):48–53
4. Bennis M, Simsek M, Czulwik A, Saad W, Valentin S, Debbah M (2013) When cellular meets WiFi in wireless small cell networks. *IEEE Commun Mag* 51(6):44–50
5. Zhang H, Jiang C, Beaulieu NC, Chu X, Wen X, Tao M (2014) Resource allocation in spectrum-sharing OFDMA femtocells with heterogeneous services. *IEEE Trans Commun* 62(7):2366–2377
6. Bennis M, Perlaza SM, Blasco P, Han Z, Poor HV (2013) Self-organization in small cell networks: a reinforcement learning approach. *IEEE Trans Commun* 12(7): 3202–3212
7. Zhang H, Jiang C, Beaulieu NC, Chu X, Wang X, Quek T (2015) Resource allocation for cognitive small cell networks: a cooperative bargaining game theoretic approach. *IEEE Trans Wirel Commun* 14(6):3481–3493
8. Hong X, Wang J, Wang C, Shi J (2014) Cognitive radio in 5G: a perspective on energy-spectral efficiency trade-off. *IEEE Commun Mag* 52(7):46–53

9. Huang L, Zhu G, Du X (2013) Cognitive femtocell networks: an opportunistic spectrum access for future indoor wireless coverage. *IEEE Wirel Commun* 20(2):44–51
10. Chen X, Zhao Z, Zhang H (2013) Stochastic power adaptation with multiagent reinforcement learning for cognitive wireless mesh networks. *IEEE Trans Mob Comput* 12(11): 2155–2166
11. Wang W, Yu G, Huang A (2013) Cognitive radio enhanced interference coordination for femtocell networks. *IEEE Commun Mag* 51(6):37–43
12. Hu D, Mao S (2012) On medium grain scalable video streaming over femtocell cognitive radio networks. *IEEE J Sel Areas Commun* 30(3):641–651
13. Urgaonkar R, Neely MJ (2012) Opportunistic cooperation in cognitive femtocell networks. *IEEE J Sel Areas Commun* 30(3):607–616
14. Cheng S, Ao W, Tseng F, Chen K (2012) Design and analysis of downlink spectrum sharing in two-tier cognitive femto networks. *IEEE Trans Veh Technol* 61(5):2194–2207
15. Wang X, Ho P, Chen K (2012) Interference analysis and mitigation for cognitive-empowered femtocells through stochastic dual control. *IEEE Trans Wirel Commun* 11(6): 2065–2075
16. Xie R, Yu FR, Ji H, Li Y (2012) Energy-efficient resource allocation for heterogeneous cognitive radio networks with femtocells. *IEEE Trans Wirel Commun* 11(11): 3910–3920
17. Le L, Niyato D, Hossain E, Kim DI, Hoang DT (2013) QoS-aware and energy-efficient resource management in OFDMA femtocells. *IEEE Trans Wirel Commun* 12(1): 180–194
18. Zhang H, Jiang C, Mao X, Chen H (2016) Interference-limit resource allocation in cognitive femtocells with fairness and imperfect spectrum sensing, accepted. *IEEE Trans Veh Technol* 65(3):1761–1771
19. Zhang H, Nie Y, Cheng J, Leung VCM, Nallanathan A (2017) Sensing time optimization and power control for energy efficient cognitive small cell with imperfect hybrid spectrum sensing. *IEEE Trans Wirel Commun* 16(2):730–743
20. Liang Y, Zeng Y, Peh ECY, Hoang A (2008) Sensing-throughput tradeoff for cognitive radio networks. *IEEE Trans Wirel Commun* 7(4):1326–1337
21. Ng DWK, Lo ES, Schober R (2012) Energy-efficient resource allocation in multi-cell OFDMA systems with limited backhaul capacity. *IEEE Trans Wirel Commun* 11(10):3618–3631
22. Xiong C, Li GY, Liu Y, Chen Y, Xu S (2013) Energy-efficient design for downlink OFDMA with delay-sensitive traffic. *IEEE Trans Wirel Commun* 12(6):3085–3095
23. Boyd S, Vandenberghe L (2004) *Convex optimization*. Cambridge University Press, Cambridge
24. Chen Y, Zhao Q, Swami A (2008) Joint design and separation principle for opportunistic spectrum access in the presence of sensing errors. *IEEE Trans Inf Theory* 54(5): 2053–2071
25. Jiang C, Chen Y, Gao Y, Liu KJR (2013) Joint spectrum sensing and access evolutionary game in cognitive radio networks. *IEEE Trans Wirel Commun* 12(5):2470–2483
26. Xie R, Yu FR, Ji H (2012) Dynamic resource allocation for heterogeneous services in cognitive radio networks with imperfect channel sensing. *IEEE Trans Veh Technol* 61(2):770–780
27. Almalfouh SM, Stuber GL (2011) Interference-aware radio resource allocation in OFDMA-based cognitive radio networks. *IEEE Trans Veh Technol* 60(4):1699–1713
28. Wong CY, Cheng R, Lataief K, Murch R (1999) Multiuser OFDM with adaptive subcarrier, bit, and power allocation. *IEEE J Sel Areas Commun* 17(10):1747–1758
29. Kang X, Zhang R, Motani M (2012) Price-based resource allocation for spectrum-sharing femtocell networks: a stackelberg game approach. *IEEE J Sel Areas Commun* 30(3): 538–549
30. Son K, Lee S, Yi Y, Chong S (2011) Refim: a practical interference management in heterogeneous wireless access networks. *IEEE J Sel Areas Commun* 29(6):1260–1272
31. Shen Z, Andrews JG, Evans BL (2005) Adaptive resource allocation in multiuser OFDM systems with proportional rate constraints. *IEEE Trans Wirel Commun* 4(6):2726–2737

32. Further advancements for E-UTRA, physical layer aspects, 3GPP Std. TR 36.814 v9.0.0, 2010
33. Tao M, Liang Y-C, Zhang F (2008) Resource allocation for delay differentiated traffic in multiuser OFDM systems. *IEEE Trans Wirel Commun* 7(6):2190–2201

Further Reading

1. Hsiung CY, Mao GY (1998) *Linear algebra*. Allied Publishers